Temporal and environmental significance of microbial lamination: insights from Recent fluvial stromatolites in the River Piedra, Spain

CONCHA ARENAS[1*], BRIAN JONES[2]

[1] *Division of Stratigraphy, Department of Earth Sciences, University of Zaragoza. 50009 Zaragoza, Spain*

[2] *Department of Earth and Atmospheric Sciences, University of Alberta. Edmonton, Alberta T6G 2E3, Canada*

*Corresponding author. E-mail address: *carenas@unizar.es*.

Temporal and environmental significance of microbial lamination: insights from Recent fluvial stromatolites in the River Piedra, Spain

CONCHA ARENAS[1*], BRIAN JONES[2]

[1] *Division of Stratigraphy, Department of Earth Sciences, University of Zaragoza. 50009 Zaragoza, Spain*

[2] *Department of Earth and Atmospheric Sciences, University of Alberta. Edmonton, Alberta T6G 2E3, Canada*

*Corresponding author. E-mail address: *carenas@unizar.es*.

Associate Editor - Cathy Hollis

Short Title – Temporal and environmental significance of microbial lamination

----

ABSTRACT

Despite extensive research, the environmental and temporal significance of microbial lamination is still ambiguous because of the complexity of the parameters that control its development. A 13 year monitored record of modern fast-accreting calcite stromatolites (mean 14 mm/year) from artificial substrates installed in rapid-flow in the River Piedra (NE Spain) allows comparison of the sedimentological attributes of successive six-month depositional packages with the known climatic, hydrophysical, and hydrochemical parameters of the depositional system. The stromatolites are formed of dense, porous and macrocrystalline composite laminae. The dense and porous composite laminae, which are composed of two to eight laminae consisting largely of calcified cyanobacteria, are characterized by: (i) dense composite laminae, up to 15 mm thick, mostly with successive dense laminae and minor alternating dense and porous laminae, and (ii) porous composite laminae, up to 12 mm thick, consisting mainly of porous laminae alternating with thinner dense laminae. Most of the dense composite laminae formed during the warm periods (April to September), whereas most of the porous composite laminae developed in the cool periods (October to March). Each dense and porous composite lamina represents up to or slightly longer than six months. The alternation of these two types of composite laminae parallels seasonal changes in temperature. The dense and porous laminae result from shorter (e.g., intraseasonal) variations in temperature, insolation and hydrological conditions. The macrocrystalline laminae, with crystals >100 µm long, occur isolated and grouped into composite laminae up to 1.7 mm thick. Their occurrence suggests the absence or poor development of microbial mats over periods of weeks to several months. Thus, stromatolite lamination can record different-order, periodic and non-periodic changes in magnitude of

environmental parameters over a single year. These results hold important implications for the temporal and environmental interpretation of lamination in microbial structures.

Keywords: Environmental parameters, fluvial carbonate deposits, microbial and non-microbial laminae, seasonal and intraseasonal variations, stromatolite lamination, textural cyclicity

INTRODUCTION

The analysis of laminations in ancient microbialites has been the focus of many studies (Monty, 1976; Casanova, 1994; Zamarreño et al., 1997; Riding, 2000; Suárez-González et al., 2014). Interpretation of the environmental and temporal significance of these laminations is, however, commonly ambiguous because of the complexity of the physical, chemical and biological parameters that collectively control their development (Hofmann, 1973; Seong-Joo et al., 2000; Storrie-Lombardi & Awramik, 2006; Petryshyn et al., 2012). The situation is further complicated by diagenetic processes that may modify the original textural (Park, 1976; Golubić et al., 2008).

Hofmann (1973) noted that stromatolite lamination could be related to several cycles of different duration (e.g., daily, short tidal cycles, monthly or seasonal), the origin of which could be astronomic (gravitational and climatic), geologic, or biologic. Stable-isotope ($\delta^{13}C$ and $\delta^{18}O$) records from laminated microbialites commonly reveal climatic and associated hydrological changes on various time scales (i.e. seasonal and pluriseasonal; Andrews & Brasier, 2005; Kano et al., 2007; Kremer et al., 2008; Osácar et al., 2013; Tang et al., 2014; Arenas et al., 2015). Although the recognition of such changes based on textural attributes and/or thicknesses of the laminae is not always straightforward (e.g. Kremer et al., 2008;

Brasier et al., 2011), daily or nyctohemeral laminations have been identified in some stromatolites on the basis of textural variations (Gebelein, 1969; Monty, 1978; Wright & Wright, 1985).

The role of microbes and extracellular polymeric substances (EPS) on carbonate precipitation in modern microbial mats has been reviewed by Dupraz et al. (2009) and Spadafora et al. (2010). Under rapid CO_2 degassing conditions, like those found in fast-flow and agitated water conditions, carbonate precipitation is more influenced by physico-chemical processes than in still water conditions where microbial CO_2- and HCO_3^--uptake may be more important (Merz-Preiß & Riding, 1999; Arp et al., 2001). In terms of cyanobacterial calcification, sheath encrustation dominates in fast-flowing conditions, whereas sheath impregnation dominates where calcification is slower (Merz-Preiß & Riding, 1999). Nonetheless, precipitation below the surface mat related to other bacteria that degrade organic matter is also important. There, lamina formation has also been attributed to degradation of cyanobacterial biomass, phototrophic sulphide oxidation and sulphate reduction (Vasconcelos et al., 2013). Grain trapping and binding by microbes are also important, particularly in the formation of coarse-grained, agglutinated stromatolite laminations (Riding, 2000; Reid et al., 2000; Suárez-Gonzaléz et al., 2014).

Despite the varied factors and processes involved in the origin of laminations, the “petrographic” result is quite simple and similar in most modern and fossil examples (Monty, 1976). Monty (1976) defined different types of laminations in stromatolites on the basis of the cyclic or recurring pattern of the laminae that are defined by their colour, crystal size and porosity. In most ancient and recent fine-grained microbialites, the most common arrangement is an alternation of dense, dark laminae and porous, light laminae that has commonly been considered a yearly record. In many cases, this yearly record reflects seasonal variations in precipitation and/or temperature that have been described in continental

(Casanova, 1994; Zamarreño et al., 1997; Matsuoka et al., 2001; Ihlenfeld et al., 2003; Kano et al., 2003, 2004; O'Brien et al., 2006; Brasier et al., 2011) and marine environments (Kremer et al., 2008; Tang et al., 2014). These parameters can also operate over other time spans (e.g. Petryshyn et al., 2012) and other astronomic factors may also influence marine microbialite lamina formation (e.g., tidal cycles, Hofmann, 1973).

The accretion rates of oncolites and stromatolites growing in modern fluvial carbonate systems are high (4 to 14 mm/year in stromatolites) with a variety of laminae commonly forming within several months (Ordóñez et al., 1980; Gradziński, 2010; Vázquez-Urbez et al., 2010; Manzo et al., 2012; Arenas et al., 2014). The cyclicity of such laminae and their temporal and environmental significance, however, have not been fully explained.

This paper focuses on stromatolites that form under rapid flow conditions in a fluvial environment (i.e. tufa system). It is based on deposits that accumulated on artificial substrates placed in the River Piedra (northeastern Spain) from 1999 to 2012 (Fig. 1A). During this 13-year time span, the deposits were examined and their thicknesses measured every six months (at the end of winter and at the end of summer). This information allows correlation of the lamina/stromatolite development with the known climatic, hydrochemical, and hydrophysical attributes of the system.

Using information collected from the River Piedra, this paper (i) describes the main structural and textural attributes of the laminae in the stromatolites and discusses the factors/parameters that controlled their formation, and (ii) relates the variations in textural features and the different styles of lamina to environmental parameters that operate at different time scales in response to a variety of intrinsic and extrinsic factors. Integration of all the available information provides a model for the development of laminae in fluvial stromatolites and allows discussion on their temporal significance. These results also carry important implications for the interpretation of laminae found in other microbial structures.

LOCATION, GEOLOGICAL, CLIMATIC AND HYDROLOGICAL SETTINGS OF THE STUDIED SITE

Geographical, geological and climatic context

The River Piedra is a 41 km long indirect tributary of the River Ebro that flows south to north across the Iberian Range, which is located in the northeastern part of the Iberian Peninsula (Fig. 1A). The Iberian Range is an Alpine intraplate fold belt with thick Mesozoic carbonate formations that are widespread and house karstic aquifers that feed the entrenched drainage network. Extensive fluvial tufa sequences formed during the Quaternary in relation to karstic dynamics (Sancho et al., 2015). As in the River Piedra, tufa is still actively forming in many of these valleys.

The River Piedra is fed mainly by water from an aquifer in Lower Jurassic and Upper Cretaceous limestones and dolostones (Servicio Geológico de Obras Públicas, 1990). The most important natural springs are near Cimballa (Fig. 1B), with a mean discharge rate of 1.4 m^3/s (data from *Confederación Hidrográfica del Ebro*, http://195.55.247.237/saihebro/). From October 1999 to September 2012, the mean annual discharge was ~ 1.06 m^3/s (data compiled from *Confederación Hidrográfica del Ebro* by Arenas et al. 2014). Maximum discharge is in the winter, whereas the minimum discharge occurs during the summer, although the river has never gone dry.

The climate of the region is continental Mediterranean with strong seasonal contrasts in temperature and precipitation. From October 1999 to September 2012, the mean annual air temperature was 13.1°C. Air temperature was highest in July and August (mean monthly temperature of 21.7°C to 25ºC) and lowest between December and February (mean monthly temperature of 2.4ºC to 7ºC). The mean annual rainfall was 397.4 mm, irregularly distributed through the year, with maxima in April, May and October (air temperature and precipitation data provided by *Agencia Estatal de Meteorología*, values averaged from the La Tranquera and Milmarcos meteorological stations, approximately 700 and 1050 m above sea-level, respectively). Herein, the "warm" period includes spring and summer (21st March to 22nd September), whereas the "cool" period includes autumn and winter (22nd September to 21st March).

During the Quaternary, incision of the River Piedra created a fluvial valley with several topographical breaks that favoured tufa deposition from the Pleistocene to present. The Quaternary tufa deposits are distributed along the lower reach of the river upstream of its entrance into the La Tranquera reservoir (Vázquez-Urbez et al., 2011, 2012; Sancho et al., 2015). Within and close to the Monasterio de Piedra Natural Park, waterfalls 12 to 35 m high are present. Modern tufa is being deposited in the park at high rates in various fluvial environments (Vázquez-Urbez et al., 2010).

Hydrochemistry

The water of the River Piedra is of the HCO_3-Ca type at the headwaters, changing towards a HCO_3-(SO_4)-Ca type downstream (based on biannual analysis from October 1999 to September 2012, Arenas et al., 2014). The calculated partial pressure of CO_2 (pCO_2) was highest at the headwaters and decreased downstream due to CO_2 outgassing, especially at topographic breaks. The river water was in equilibrium or oversaturated with respect to calcite. The calculated saturation index with respect to calcite (SIc) and the PWP rates (the inorganic precipitation rate for calcite calculated using the rate law of Plummer et al., 1978) show seasonal fluctuations, with the higher values during the warm periods and lower values during the cool periods (Arenas et al., 2014).

METHODS

This research is based on the sedimentary deposits that accumulated on artificial limestone tablets (25 x 16 x 2 cm) that were installed at seven fast-flowing water (2.3 < m/s > 0.9) sites along the River Piedra close to and in the Monasterio de Piedra Natural Park (Fig. 1B and C, Table 1). These deposits accumulated between November 1999 and September 2012. At each site, monitoring (every three and six months, depending on parameters) of the physical flow characteristics (water velocity and depth, every three months), water chemical and isotopic composition, and isotopic composition and structural and textural attributes of deposits was made, and the six-month deposition rates were measured (Tables 1 and 2). Water temperature was also measured instantly every three months at each site. A continuous hourly recording of water temperature was conducted from July 2007 to September 2012 using two temperature recorders (HOBO Pro V2; Onset, Cape Cod, Massachussets, USA). Climatic (air temperature and precipitation) and hydrological (discharge) data over the 13-year period were obtained from *Agencia Estatal de Meteorología* and *Confederación Hidrográfica del Ebro*. Results concerning deposition rates, hydrochemistry and stable isotope composition are provided by Vázquez-Urbez et al. (2010), Arenas et al. (2014) and Osácar et al. (2016).

The tablets, which were installed parallel to the river bed, were removed at the end of March and end of September of each year in order to measure the thickness of the accumulated sediment for every cool and warm period. After measurement, the tablets were returned to their original position. The details of the procedure are described by Vázquez-Urbez et al. (2010).

During the 13-year study, each tablet was replaced with new ones every three to four years. Once removed, the tablets were cut perpendicular to the accumulation surface, and the six-month intervals were identified on cross-sections by plotting the successive measurements of thickness that had been taken every six months. Thin sections were then made from these sections after impregnation with epoxy resin. The thin sections were made at the *Servicio General de Apoyo a la Investigación-SAI* facilities of the University of Zaragoza (Spain). Fracture samples (up to 1.5 x 1 x 0.5 cm) taken from different six-month deposits were used for scanning electron microscopy (SEM) analyses. These samples were coated with gold or carbon. The analyses were done on a JEOL JSM 6400 (JEOL Limited, Tokyo, Japan) and a Carl Zeiss MERLIN™ (Carl Zeiss Group, Jena, Germany) at the *Servicio General de Apoyo a la Investigación-SAI* of the University of Zaragoza, and a JEOL 6301FXV (Carl Zeiss Group, Jena, Germany) at the Department of Earth and Atmospheric Sciences of the University of Alberta (Canada), that were typically operated at 3-5 kV and 150-500 pA.

The mineralogy of the deposits on tablets was determined by X-ray diffraction using a Phillips PW 1729 diffractometer (Phillips Analytical, Almelo, Netherlands) at the Crystallography and Mineralogy Division of the University of Zaragoza.

TERMINOLOGY

Herein, the term "microbialite", following the definition of Burne & Moore (1987, pp. 241–242), is used for "…organosedimentary deposits that have accreted as a result of a benthic microbial community trapping and binding detrital sediment and/or forming the locus of mineral precipitation". Laminated microbialites that grow attached to the sedimentary surface are termed stromatolites, whereas those that grow unattached are termed oncolites (cf. Riding, 1991).

A biofilm consists of a microbial community that is embedded in extracellular polymeric substances (EPS) (Rosenberg, 1989; Neu, 1996; Decho, 2010). The EPS is a hydrogel that allows microbes to attach themselves to substrates while buffering them from the immediate extracellular environment (Decho, 2010). Microbial mats involve stratification of the microbial populations into several layers (Krumbein et al., 2003, p. 13) and may therefore be considered as complex biofilms (Stolz, 2000). Herein, the term “microbial/cyanobacterial mat” is used in a general sense and refers to microbial/cyanobacterial populations that coat the substrate, independent of the complexity of their internal structure.

Following Preiss (1972) and Walter (1972), who defined a lamina as “the smallest unit of layering”, the term “lamina” herein refers to a layer with a largely uniform texture that is ≤ 1 cm thick (Fig. 2). Herein, very thin laminae, up to 100 µm thick, are named microlaminae.

Following Arenas et al. (2007, 2015), the term “composite lamina” refers to a group of two or more laminae that is distinguished from the underlying and/or overlying deposits by changes in lamina thickness, colour and/or texture (Fig. 2). The laminae forming the composite laminae may have the same or different texture. Each composite lamina is 1 to 15 mm thick.

A monocrystal, or single crystal, “…is a crystalline solid in which the crystal lattice of the entire sample is continuous and unbroken to the edge of the sample with no grain boundaries” (Meldrum & Cölfen, 2008, p. 4336). A mesocrystal (abbreviation for a “mesoscopically structured crystal”) is built up of nanocrystals that “…are aligned in a common crystallographic register” (Meldrum & Cölfen, 2008, p. 4343). A mesocrystal is equivalent to aggregate crystals, composite crystals, and polycrystalline crystals (cf. Peng & Jones, 2013, and references therein). Nanoparticles are (sub)spherical particles with no evidence of crystal faces and/or edges, smaller than 1 µm (cf. Peng & Jones, 2013).

Micrite and spar are used for calcite crystals that are up to *ca.* 4 µm and > 4 µm, respectively. Crystals, one hundred to several hundred µm long, are named macrocrystals.

SEDIMENTOLOGICAL CHARACTERISTICS OF THE FLUVIAL TUFA SYSTEM

In the River Piedra, calcite deposition is first detected ~ 8 km downstream of the main springs and then increases significantly downstream close to and within the park, coinciding with an increase in riverbed slope (Arenas et al., 2014). Carbonate sedimentation takes place in various depositional environments that are defined by the morphological features of the riverbed (e.g., bed slope), physical flow characteristics (e.g., water velocity and depth), and substrate biota (e.g., floral associations and bacteria). The main facies, as described by Arenas et al. (2014), are:

A) stromatolites in fast-flowing water (> 0.9 m/s),

B) loose lime mud, phytoclasts, and oncoids in slow flowing water (< 0.8 m/s),

C) thick boundstones consisting of calcite-coated moss and macroscopic filamentous algae (green and yellow-green) in moderate flowing water (stepped waterfalls),

D) very thin and discontinuous stromatolites and boundstones consisting of calcite-coated moss and macroscopic filamentous algae (green algae) in spray and splash zones, and

E) moss and hanging-stem boundstones in vertical waterfalls, with fast vertical flow.

The sediments in these facies are formed of low-Mg calcite with minor amounts of detrital phyllosilicates, quartz and dolomite. Their deposition rates (except for the vertical waterfalls that were not measured due to the difficulty of access), from 1.3 to 14 mm/year, are largely a function of the rate of CO_2 outgassing in relation to flow conditions (Arenas et al., 2014), as in other modern tufa systems (Chen et al. 2004; Gradziński, 2010). The deposition rates in all facies are higher in the warm periods than in the cool periods. These differences were caused mainly by seasonal variations in temperature-dependent parameters, such as water saturation with respect to calcite, the development of flora and prokaryotes and the associated photosynthetic activity. Thus, tufa deposition rates in this river are controlled by both physicochemical and biological processes (Arenas et al., 2014).

The primary focus of this study are the stromatolites (facies A) that developed in the fast-flowing water (0.9 to 2.3 m/s) on substrates with inclinations of 10 to 75º and water 2 to 9 cm deep (Tables 1 and 2). In all settings, brown to bluish grey bacterial mats cover the stromatolite surface (Fig. 3B and F). They are found in the following settings:

(1) Rapids and small waterfalls that are devoid of macrophytes, where the stromatolites form thick, laterally extensive deposits (Fig. 3A to D), with deposition rates of 6.7 to 16.5 mm/y, and mean values of 9.5 mm/6 months in warm periods and 4.4 mm/6 months in cool periods (Table 1), and

(2) Stepped waterfalls, where moss and filamentous algae dominate (Fig. 3E) and water flow is variable. The stromatolites (Fig. 3F, G and H) develop mostly in the high flow zones where they are interbedded with moss and algal boundstones (Fig. 3F). Deposition rates, which include the moss and algal boundstones (facies C) and stromatolites (facies A), are 7.8 to 13.1 mm/y, with mean values of 6.9 mm/6 months in the warm periods and 3.6 mm/6 months in the cool periods (Table 1).

RESULTS

Types of laminae

In hand samples, the stromatolites that formed on the tablets between 1999 and 2012 (Table 1) are characterized by slightly undulatory, convex to multiconvex, or flat, laterally persistent laminae that are up to 2.5 mm thick (Figs 3C, 3D, 3G, 3H and 4). Most stromatolites are formed of alternating dense and porous composite laminae (Fig. 4 and Table 3). Throughout the stromatolites there are laminae formed of calcite macrocrystals that can be isolated or grouped into composite laminae.

Dense composite laminae

In thin section, it is evident that the dense, dark-coloured, composite laminae, 3.5 to 15 mm thick, are formed of well defined laminae that have slightly undulatory, convex or, less commonly, flat bounding surfaces (Figs 4 and 5). Each dense composite laminae is formed of up to eight laminae (Fig. 5A and B). Successive, dense composite laminae can be separated by a thin macrocrystalline lamina or an erosional surface (Fig. 4A and C). The dense composite laminae are formed of laterally continuous, micrite and spar calcite laminae that are 0.5 to 2.5 mm thick, but with some up to 5 mm thick. Although the dense and porous laminae can alternate, successive dense laminae can also form a dense composite laminae. In general, the dense laminae are usually thicker than the porous laminae. Some dense composite laminae include up to 100 microlaminae. Thin macrocrystalline laminae, 0.1 to 0.3 mm thick, can be included within the dense composite laminae (Fig. 5A and B).

Porosity, generally < 5% (visual estimate from thin section), is mainly mouldic after aquatic worms (pores with rounded and elliptical cross-sections) and insects (pores with irregular or flat base and convex upward top) with pores < 0.5 mm in diameter. These cavities are typically aligned parallel to the laminae. Growth framework porosity is very low.

Porous composite laminae

In the porous composite laminae, which are 2 to 7.5 mm thick (exceptionally 12 mm) with undulatory bounding surfaces (Fig. 5), the laminae can be difficult to identify because of the high porosity (Fig. 4). These light-coloured (in thin section) composite laminae, consisting of micrite and spar calcite, are composed of two to five laminae, each being submillimetre to 2 mm thick, that have irregular and undulatory bounding surfaces and variable lateral continuity. Most porous composite laminae are formed of alternating dense laminae and thicker porous laminae (Fig. 5). The boundary between the porous and dense laminae can be gradual or sharp.

Porosity, up to 15% (visual estimate from thin section), is a conspicuous feature of the porous composite laminae. Cavities, submillimetres to centimetres across, of varying shape are present, both parallel to lamination and at random (Fig. 5). The following types are present:

(i) growth framework porosity (uneven and patchly, between filamentous bodies and microbial structures),

(ii) mouldic porosity, with pores that are rounded (from worms) or have an irregular, flat base and rounded top (from insects), < 1 mm in diameter; most of the latter are aligned parallel to lamination or randomly,

(iii) irregular cavities, mostly random but with some parallel to lamination, that may be enlarged mouldic porosity (vuggy porosity) and/or enlarged framework porosity.

Macrocrystalline composite laminae

The macrocrystalline composite laminae, 1 to 1.7 mm thick, typically have flat bases and slightly undulatory tops. These laminae are formed of elongate crystals that are perpendicular to the depositional surface and in the thickest laminae can be seen with the unaided eye (Fig. 4A). Microscopically, these composite white to cream-coloured laminae consist of up to three macrocrystalline laminae that have flat and slightly undulatory boundaries (Fig. 5A). The contact between consecutive laminae is an irregular surface. In rare cases, a laterally discontinuous micrite lamina, 0.2 to 0.8 mm thick, is present between successive macrocrystalline laminae. These micrite laminae include microbial calcite filamentous bodies and clumps of calcite crytals. Porosity is low and mainly interparticle in nature. The macrocrystalline composite laminae are less common than the two other types of composite laminae.

Dense, porous and macrocrystalline laminae

The dense, porous, and macrocrystalline laminae that form the composite laminae in the stromatolites are characterized by the following features (Table 3):

(i) Dense laminae, 0.2 to 5 mm thick, consisting of micrite and spar calcite, are formed of tightly-packed calcified filamentous microbes, arranged as semi-parallel bodies and/or fan-like structures, that are oblique to (sub)perpendicular to the depositional surface (Figs 5, 6A and 6B). Commonly, each lamina is defined by a palisade of calcified filamentous microbes. Consecutive laminae, which are distinguished from each other by colour, porosity, and crystal size, are separated by sharp to gradual contacts (Figs 5A and 6A). Many laminae are characterized by an upward decrease in porosity. Microlamination is conspicuous in some of the dense laminae (Fig. 6C).

(ii) Porous laminae, 0.5 to 2 mm thick, formed of micrite and spar calcite, are characterized by loosely-packed calcified filamentous microbes that are typically arranged like those in the dense laminae (Fig. 5A and B). Growth framework porosity is high because of the wide spacing between the filaments. The microbial structures (palisades made of semi-parallel bodies and fan-like bodies) define microlaminae that are 30 to 100 μm thick and have variable porosity (Figs 5, 6D and 6E).

(iii) Macrocrystalline laminae, 0.1 to 1.3 mm thick, are of variable lateral extent and have sharp flat and convex-up bases and irregular, flat and convex-up tops. Each lamina consists of closely packed elongate calcite crystals that are (sub)perpendicular to the depositional surface and widen upward to produce a fence-like structure (Figs 5A and 6F). The thickness of individual lamina is defined largely by the length of the formative crystals. These macrocrystalline laminae are commonly found at the base of tablet deposits (Figs 5 and 6F), at the boundaries between dense and porous composite laminae (Fig. 6F) and over irregular erosional surfaces (Fig. 6B).

Elongate crystals like those in the macrocrystalline lamine are found on top of some cavities formed after the decay of organisms (mainly insects and worms). In such cases, the crystals form lenses up to 0.7 mm thick that mimic the convex-up shape of the organisms (Fig. 6G and H).

Cyanobacterial structures and calcification pattern in the dense and porous composite laminae

Cyanobacterial fabrics and calcification pattern

As shown by Vázquez-Urbez et al. (2010), Arenas et al. (2014), and Berrendero et al. (2016), the calcified filaments found in the dense and porous composite laminae (Figs 5 and 6) are tubes that formed around the filamentous microbes prior to their decay (Figs 7, 8A and 8B). Similar calcitic tubes have been described from other tufa stromatolites (Merz-Preiß & Riding, 1999; Pentecost, 2005; Golubić et al., 2008).

Relative to the depositional surface, the tubes are perpendicular, subperpendicular, oblique, and less frequently subhorizontal. Although all orientations can be found in one lamina, perpendicular and subperpendicular forms usually dominate in the upper part of a lamina (Fig. 7A and B). There are two basic arrangements of the tubes:

(a) Closely packed parallel tubes, with most being subperpedicular to the depositional surface (Fig. 7C). This arrangement is most common in the dense laminae and particularly in the uppermost laminae of the dense composite laminae.

(b) Oblique and subperpendicular tubes, with fewer subhorizontal tubes, that can be at random but also arranged as isolated or adjacent fan-shaped bodies (i.e. domes). In general, this style is most common in the porous laminae (Fig. 7D).

Individual laminae can be formed entirely of a single arrangement style of tubes or grade vertically from style (b) at the base to style (a) at the top (Fig. 7B).

The tubes typically have an inner diameter of 6.0 to 7.5 µm and walls 3 to 8 µm thick but up to 17 µm thick in some specimens (Figs 7E, 7F and 8). The inner diameter is consistent with the diameter of *Phormidium incrustatum,* as determined through morphological and DNA analyses of living cyanobacterial mats (Berrendero et al., 2016). This is the dominant cyanobacterial species (> 97 %) in the fast-flowing areas of the River Piedra (Berrendero et al., 2016). Locally, rare (1-3 %) smaller tubes (2-3 µm long, inner diameter 2-3 µm, walls < 2 µm thick), that are probably *Leptolyngbya* sp. (Fig. 7E and F) are present (Berrendero et al., 2016). Despite calcification, the sheaths of these microbes are rarely preserved. The matrix between the cyanobacterial tubes consists of calcite crystals of variable sizes and shapes, extracellular polymeric substances (EPS), diatoms, rare non-calcified bacterial filaments, and scattered allochthonous phyllosilicates and quartz grains (Fig. 7F).

The calcite crystals that form the tubes are up to 15 µm long. The inner part of the walls are formed of nanoparticles, nanocrystals, and small mesocrystals (Fig. 8A to C). Commonly, these subspherical, rod-shaped, and rhombohedral crystals (Fig. 8C) are randomly arranged or are aligned forming rods. The walls of the small-diameter tubes are formed largely of nanocrystals. Although the walls of some large-diameter tubes are formed entirely of nanocrystals/nanoparticles (Fig. 8D), most are characterized by an outward increase in crystal size and large crystals commonly dominate. These include: (i) rhombohedral mesocrystals (Fig. 8B, C, E and F), (ii) trigonal mesocrystals (Fig. 8G) that are most common in the outer parts of the tubes, and (iii) other polyhedra and irregular forms, commonly mesocrystals (Fig. 8A and H).

EPS occur as: (i) films in the inner part of walls of the tubes (Fig. 9F), (ii) strands between crystals (Fig. 8G and H) inside the tubes and between the tubes (Fig. 8I) and (iii) films that cover crystals in and between the tubes. Nanocrystals/nanoparticles and rhombohedra that are isolated or grouped together are commonly embedded in the EPS.

Diverse species of diatoms (mainly pennate, and less commonly centric) both with intact and broken frustules, are ubiquitous inside and between the tubes. Diatoms are closely associated with EPS and nanoparticles. Diatoms can be uncoated or coated with EPS and/or calcite crystals (Fig. 8J). Calcified and uncalcified bacterial filaments, mostly < 0.5 μm wide, and associated nanocrystals and nanoparticles, are commonly associated with the EPS (Fig. 8C).

Differences between the dense and porous laminae

The contrasts between the dense and porous laminae are related largely to the density and arrangement of the tubes in each laminae (Fig. 7A to D). The dense laminae, for example, commonly contain more palisades formed of (sub)perpendicular tubes (Fig. 7A), whereas the porous laminae have more domes and microlaminae (Fig. 7B).

Calcification of the tubes in the dense and porous laminae share many common features (Figs 9 and 10). In some cases, however, the dense laminae have a higher density of tubes (Fig. 9A and B) and the walls of tubes are thicker (Fig. 9C to F) than in the porous laminae (Fig. 10). Although there are no systematic differences in crystal size and shape between the dense and porous laminae, larger crystals seem to dominate in some of the porous composite laminae. In general, the tubes associated with the warm period deposits (dense composite laminae) exhibit smaller crystals than those in the cool period deposits (Fig. 9D and E compared to Fig. 10D and E). In some cases, the crystals on the outermost part of walls of the tubes in the cold period deposits are better formed, as are the crystals between these tubes (Fig. 10D and E).

Texture of macrocrystalline composite laminae

In each macrocrystalline lamina, the crystals have a cone-like shape that widens upward (up to 100-120 μm wide), with an approximately rounded cross-section; most crystals narrow at the top and have rounded terminations (Fig. 11A, B, D and F). The length of the crystals (0.1 to 1 mm long) may equal the thickness of the laminae, but it can be highly variable. Each elongate crystal is a mesocrystal (Fig. 11C and D). Cross-sections of the mesocrystals are structureless (Fig. 11C) apart from pores (1-2 µm across) that might correspond to bacterial moulds. These pores are also visible on the upper part of some of the crystals. In some examples, the mesocrystals may have developed from the calcite overgrowths that originally formed around the cyanobacteria tubes (Fig. 11D). The outer surfaces of the mesocrystals exhibit mostly rhombohedral crystals (Fig. 11C to E). Although some filamentous bacteria, 0.1 µm wide, are evident on the crystal surfaces, there is little evidence of EPS.

In some macrocrystalline laminae, the mesocrystals are mixed with subhorizontal and/or oblique cyanobacterial tubes and encompass EPS. This feature is common in the vertical passage from macrocrystalline to dense laminae (Fig. 11F).

Lamination pattern. Temporal significance of lamination in the River Piedra stromatolites

Systematic monitoring of stromatolite growth and sediment accumulation in the River Piedra provides a basis for interpreting the laminae in terms of their temporal and environmental significance. Most stromatolites in the River Piedra are characterized by alternating porous and dense composite laminae, which are equivalent to the "alternating composite lamination" as defined by Monty (1976). Following the terminology of Monty (1976), each composite lamina in the River Piedra stromatolites includes: (i) simple repetitive lamination (e.g., successive dense laminae, Fig. 5A and B) and/or (ii) simple alternating lamination (e.g., porous and dense laminae, Fig. 5A and B).

Deposits formed during the warm periods, from April to September, with mean thickness of 9.5 mm/6 months, are composed largely of a dense composite lamina, and, in some cases, two dense composite laminae. In some deposits, a porous composite lamina (either all or part of it) underlies the dense composite laminae (Fig. 5A, warm 06 record). In contrast, deposits that accumulated during the cool periods, from October to March, with mean thickness of 4.4 mm/6 months, consist of a porous composite lamina and, in some cases, a thin, dense composite lamina (either all or part of it) at the base (Fig. 5A). In other words, in a few cases, the dense composite lamina of the warm period may extend into the beginning of the next cool period, and the porous composite lamina of the cool period into the beginning of the next warm period. These features suggest that the six-month periods considered in this study (i.e. "astronomical seasons") are very close to the actual cycles of climate through the year (i.e. "meteorological seasons"). Thus, each dense or porous composite lamina represents a time period that is probably a few months to six months long, though in some cases it can be slightly longer than six months.

A warm period deposit can consist of a couplet that records deposition in early spring (porous composite lamina) and deposition in late spring and summer (dense composite lamina). Similarly, a cool period deposit may record deposition in the early autumn (dense composite lamina) and late autumn to winter (porous composite lamina). The processes that cause these textural changes must therefore respond to seasonal and/or pluriseasonal changes.

Given that the dense composite laminae may contain two to eight laminae and the porous composite laminae may include two to five laminae, every dense and porous laminae should represent seasonal, monthly or even shorter periods of time. The time frequency of variation in magnitude of the related environmental parameters is probably non periodic, although temporal periodicity cannot be excluded. Any other minor order of lamination (e.g., microlamination, Fig. 6C to E) should represent weekly or even shorter (e.g., daily) duration. The 90 to 100 microlaminae found in some of the dense composite laminae may be a record of daily or quasi-daily duration for each microlamina.

The macrocrystalline composite laminae and laminae occur: (i) at the base of the tablet deposits (Fig. 5A and B), irrespective of the season represented by the initial deposit (spring or autumn), (ii) at the boundary between many six-month deposits (Fig. 5A and 6E), (iii) unevenly distributed throughout the dense composite laminae in the warm deposits (Fig. 5B) and (iv) at the top of some dense laminae in the porous composite laminae (Fig. 10A). In the warm and cool deposits, the macrocrystalline laminae occur on top of erosional surfaces (Fig. 6B) and, commonly, on the upper part of the cavities that formed from the decay of insects and worms (Fig. 6G and H). From these facts, it can be concluded that the frequency and duration represented by the macrocrystalline laminae is highly variable, from a few weeks to a few, but less than six months. Some macrocrystalline composite laminae might span almost a full six-month period (e.g., Fig. 5A and B, base of each deposit).

DISCUSSION

Sedimentological significance of the different types of laminae and composite laminae: environmental control

Given that the dense and porous laminae are distinguished by the arrangement style and density of the cyanobacterial tubes and porosity, the factors that control their formation should be related to parameters that vary in magnitude over short periodic or non-periodic time spans (e.g., water temperature, flow conditions, and insolation) that influence the growth and development of the formative organisms. The main differences between the porous and dense laminae are related largely to the primary density of the organisms that inhabited the substrate (cf. Gradziński, 2010). In general, higher temperature and insolation should lead to the development of densely packed cyanobacterial filaments and, hence, denser calcite fabrics (Arp et al., 2001; Golubić et al., 2008; Kawai et al., 2009). This is consistent with the fact that in the River Piedra, calcite precipitation is more intense during warm periods than the cool periods (Arenas et al., 2014, Tables 1 and 2). Osácar et al. (2016) related the six-month cyclic $\delta^{18}O$ variation in the River Piedra stromatolites to seasonal temperature variations. In the present work, based on the correlation between the water temperature (Tw) variations and the textural variations of six-month deposits of two sites in the River Piedra, the dense and porous composite laminae correlate with high and low temperature periods, respectively (Figs 12A, 12B, 13A and 13B). The widest range of Tw variations, which occur at the end of autumn, during winter and at the beginning of spring, correlate with phases of alternating porous and dense laminae. In contrast, during periods with minimal Tw variations, which occur at the end of spring, during summer and at the beginning of autumn, more homogeneous textures of the dense composite laminae developed.

The attitude of the cyanobacterial tubes relative to their growth substrate is probably a function of flow conditions. In some tufa-depositing streams, for example, upright filament structures dominate in fast-flowing water, whereas filamentous structures with no preferred orientation grow in slow flowing water (Gradziński, 2010; Berrendero et al., 2016). It is also possible, however, that these textural differences may reflect a change in the cyanobacterial community (Berrendero et al., 2016). Thus, in a high-flow environment, like those considered herein, with one dominant cyanobacterium species (*P. incrustatum*), the variations in the arrangement style and density of cyanobacterial tubes can reflect slight changes in flow conditions. Stromatolites formed under very strong water flow in the River Piedra (e.g., in waterfalls) consist of more densely packed with mostly subvertical calcite tubes (Fig. 6A), as compared with other less intense fast-flowing zones (e.g., approximately 1 m/s) along the river (Figs 5A and 6B).

Variations in flow conditions may also contribute to changes in the pCO_2 of the water that will, in turn, affect the SIc and the PWP. This is critical because higher SIc generally lead to denser tufa fabrics (Kano et al., 2003, 2007; Gradziński, 2010; Vázquez-Urbez et al., 2010). Kawai et al. (2009) showed that the relation between biannual laminae (dense summer layer, porous winter layer) and PWP rate varied depending on the Ca content of the water. Thus, in Japanese streams with Ca > 65 mg/L, the relationship between calcite packing density and PWP became unclear. They pointed out that in such situations, it is the seasonal changes in flow rate and microbial density on the growth substrate that commonly intensifies the contrast between the bianual porous/dense laminae. In the River Piedra, Ca content is > 80 mg/L all year round (Table 2). Although there are no significant changes in mean water velocity between the warm and cool periods (Table 1), slight variations in this parameter may cause short term, higher frequency changes in porosity.

The seasonal lamination pattern consisting of dense summer and porous winter laminae appears to be reversed in some tufa stromatolite (e.g., England, Belgium and France, Kano et al. 2003; Arp et al., 2010; and references therein). Local conditions along the same stream may promote this type of change in the lamination pattern. Kano et al. (2003) found dense winter laminae and porous summer laminae in stromatolites that grew in Shirokawa Stream near the source spring, probably because calcite precipitation was high due to the low pCO_2 of the underground water during winter. The cause(s) of this change in the lamination pattern is, however, unclear. Kano et al. (2003) suggested that high water discharges during winter may increase the precipitation rate of calcite and produce dense winter laminae.

A tentative correlation between discharge variations (based on daily values) and the textural variations of two stromatolite records in the River Piedra is proposed in this work (Figs 12A, 12C, 13A and 13C). There is not a regular pattern. In some cases, however, the low and steady discharge values coincide with denser and more homogeneous textures that are formed mainly in the summer. In a few cases, the wider intraseasonal discharge oscillations, which mainly occur in the spring, appear to coincide with more porous fabrics, i.e. alternating porous and dense laminae, and even with erosional surfaces.

Periodic changes in temperature and insolation (i.e. seasonal changes) would give rise to alternating dense and porous composite laminae. In turn, shorter and likely non-periodic changes (e.g., intraseasonal variations) in temperature, insolation and/or water velocity may cause the formation of either porous or dense laminae within a composite lamina dominated by the opposite texture, either dense or porous laminae. In turn, consecutive laminae of the same texture in the River Piedra (i.e. simple repetitive lamination, cf. Monty, 1976) may result from sudden changes in the above mentioned parameters that are recorded as interruptions in the accretion process (cf. Gradziński, 2010).

Laminae and lenses formed of macrocrystalline calcite are common components of many stromatolites (cf. "sparry calcite" of Gradziński, 2010, "palisade crystal laminae" of Arp et al., 2010, "columnar calcite spar" of Brasier et al., 2011) that are formed largely of cyanobacterial tube-made laminae. Textural features of these macrocrystalline laminae and lenses in the River Piedra stromatolites suggest that these crystals probably formed as primary precipitates, as has been suggested by Gradziński (2010) and Brasier et al. (2011) in other settings.

In general, macrocrystalline laminae are thought to represent calcite precipitation at sites that lack microbial mats (Pedley, 1992, 1994; Gradzinski, 2010). Pedley (1992, 1994) considered them "winter deposits" that formed after the death of the prokaryotes in the autumn. Arp et al. (2010) also related the presence of palisade crystal laminae to the lack of cyanobacterial mats, either due to low temperature (freezing) or disruption of the growth surfaces during winter.

Some authors have related the development of large crystal laminae to lower temperature periods (Pedley, 1992), when lower SIc values commonly occur. Other authors, however, have found that large crystals form only when the SIc value is high (e.g. Arp et al., 2010), given that the length of the crystals are proportional to the SIc value (Gradzinski, 2010).

Independent of temperature, changes in SIc can also be caused by chemical changes, for instance, dilution due to heavy rainfall (cf. Auqué et al., 2014). This fact, along with the occurrence of macrocrystalline laminae and lenses within the warm period deposits in the River Piedra, suggest that temperature is not the only factor that controls the growth of the large crystals.

The lateral relation between macrocrystalline calcite and micrite (cyanobacterial-made) laminae has led to the suggestion that both textures can develop synchronously (e.g., Gradzinski, 2010; Jones & Renaut, 1994; Pedley, 2014). Pedley (2014) found that spar and micrite present in the same laminae (e.g., as in Fig. 6F in this work) formed simultaneously in fast-flowing water and suggested that their formation might be related to the presence of EPS. "Extra-EPS sites" (i.e. sites outside of the EPS influence) have faster ion supply and produce well-formed larger calcite crystals. In contrast, at "intra-EPS sites" (i.e. sites within the EPS), the precipitation rate is controlled by the external Ca ion supply rate and the biofilm requirement to chelate and relocate Ca quickly, producing smaller-crystal precipitation.

The fact that most macrocrystalline laminae and composite laminae in the River Piedra formed the initial deposits on the tablets, and occur at the boundaries between six-month period deposits and over erosional surfaces, irrespective of season, further reinforces the notion that macrocrystal precipitation is related to the absence of microbial mats. The lack of cyanobacterial development occurs: (i) on blank tablets or on insects or worms and (ii) due to interruptions of the microbial growth. The interruptions are either related to very low temperature periods, the lack of water for a short time, or erosion of the tufa surface. The lack of microbial mat implies the absence of the effects of EPS over calcium carbonate precipitation through attracting and binding Ca ions, i.e. through depleting Ca ions from the proximal surrounding environment (Kawaguchi & Decho, 2002; Dupraz & Visscher, 2005).

This circumstance favours direct and rapid precipitation of large crystals, as noted by Pedley (2014).

This view is opposite to the results of tufa precipitation obtained in laboratory systems that suggest that microbial mats are needed for $CaCO_3$ precipitation (Shiraishi et al., 2008; Rogerson et al., 2008, 2010). In the experiments by Shiraishi et al. (2008) no spontaneous precipitation occurred on microbial mat-free limestone substrates even at high calcite supersaturation conditions. Similarly, in the experiments performed by Rogerson et al. (2008) under sterilized conditions, precipitation on the bottom of the experimental flumes was not observed. It was only in the experiments with biofilms that extensive precipitation occurred. Manzo et al. (2012), in their one-year study of a fluvial tufa system in southern Italy, also indicated that no precipitation takes places where the microbial mat is absent. These observations support a biomediated origin of tufa with some type of compulsory microbiological influence needed to generate the $CaCO_3$ precipitates (Rogerson et al., 2010). Results from the River Piedra, however, suggest that macrocrystal precipitation takes place in the absence or poor development of microbial mats on the precipitation surface (i.e. forming macrocrystalline laminae). It would appear, therefore, that not all laboratory experiments can replicate what happens in the natural systems.

Factors controlling the calcification pattern of cyanobacteria in fluvial stromatolites

Studies on modern sedimentation and hydrochemistry in the River Piedra tufa system suggested that most calcite precipitation was induced by mechanical CO_2-loss, and indicated that cyanobacteria acted as substrates for calcite precipitation, with a minor contribution through photosynthetical CO_2 uptake to the stromatolite formation (Vázquez-Urbez et al., 2010; Arenas et al., 2014; Berrendero et al., 2016). This result is consistent with other experimental studies that calculated that up to 20% of calcification in *Rivularia* could be the direct result of photosynthesis, based on rates of photosynthetic CO_2 uptake with ^{14}C (Pentecost, 1975). Similarly, in other European karst streams, cyanobacterial photosynthesis accounted for 10–20% of the total Ca^{2+} loss, with the remaining Ca^{2+} loss linked to physicochemical precipitation (Shiraishi et al., 2008; Arp et al., 2010; Pentecost & Franke, 2010).

Calcite encrustation is the dominant process in cyanobacterial calcification in the stromatolites formed in fast-flowing water areas of the River Piedra (Vázquez-Urbez et al., 2010; Berrendero et al., 2016), and other recent fluvial stromatolite deposits (Merz-Preiß & Riding, 1999; Golubić et al., 2008; Pedley et al., 2009; Gradziński, 2010). Thickness variations in calcite encrustation around *P. incrustatum* of the studied deposits (2 to 12 µm) do not seem to follow any regular patterns in terms of space or time. In some cases, however, it seems that thicker encrustations developed in the warm periods, which is consistent with the higher SIc that characterize these periods (Table 2).

The lack of a distinct and persistent pattern in the thicknesses of the encrustations through time might reflect the fact that the water is oversaturated with respect to calcite throughout the year. It is possible, however, that small variations in any of the parameters that contribute to bulk SIc of water may cause slight differences in the degree of calcification (Arp et al., 2010), and thereby produce uneven changes in encrustation thickness through time. This may also explain the lack of spatial variations in the degree of calcification.

Previous studies in the River Piedra indicated that the encrustations were not characterized by any systematic patterns in crystal size or shape (Vázquez-Urbez et al., 2010; Arenas et al., 2014; Berrendero et al., 2016). In some cases, the thin encrustations are formed of irregular, anhedral calcite nanoparticles (Fig. 8C and D). In some thicker encrustations, however, smaller and/or irregular crystals occur in the inner part and the outer parts are formed of larger and/or well formed crystals (Fig. 8A and B). Analysis of numerous samples in this study confirms these results. Pedley et al. (2009) and Gradziński (2010) also noticed an outward increase in crystal size in the calcified walls that had formed around cyanobacterial tubes. In general, it is assumed that the EPS produced around the cells may have contributed to such morphological variations through microscale changes in SIc (Jones & Peng, 2014). Higher saturation levels are expected around the cell walls (Jiménez-López et al., 2011), producing small and irregular particles. Ongoing crystal precipitation around the filament progressively isolates the growth surface from cyanobacterial influence, thus decreasing the effect of EPS over calcium carbonate precipitation outward, as described above (Kawaguchi & Decho, 2002; Dupraz & Visscher, 2005). As a result, the larger and better formed crystals that develop in the external surfaces of tubes rather reflect the physicochemical conditions in the surrounding water than in the cell EPS (Jones & Peng, 2014).

Differences in crystal size and shape between encrustations formed in cool periods and warm periods in the River Piedra are even more difficult to discern (Figs 9 and 10). As noted previously (Vázquez-Urbez et al., 2010), the encrustations around the cyanobacteria formed during the cool periods are typically characterized by larger and better formed crystals than those that formed during the warm periods. This is consistent with the SIc changes of the water that are related to seasonal temperature differences (Table 2). The more abundant larger crystals in the tubes formed in the cool periods may also reflect the dominant influence of physicochemical conditions in the bulk water and lesser influence of the EPS. Nevertheless, this generality has many exceptions and contrasts with the situation in other tufas where textural changes are clearly seasonal in nature (e.g. Manzo et al., 2012).

Comparison with other examples: Temporal significance of lamination and implications for interpretation of the geological record

Most stromatolites and oncolites encompass more than one type of lamination, based on the repetition pattern and/or the textural components (Monty, 1976; Casanova, 1994; Arenas et al., 2007; Suárez-González et al., 2014) and the rank of cyclicity (Lindqvist, 1994; Seong-Joo *et al.*, 2000; Storrie-Lombardi & Awramik, 2006; Petryshyn *et al.*, 2012; Arenas et al., 2015). With respect to stromatolites, most studies have focussed on the environmental and temporal significance of the laminae based largely on their thickness and textural features (Casanova, 1994; Seong-Joo et al., 2000; Storrie-Lombardi & Awramik, 2006; Suárez-González et al., 2014). Park (1976) noted, however, the difficulty in determining the temporal significance of stromatolite laminations. Monitoring of modern coastal microbial mat surfaces, for example, has shown that millimetre-scale laminae may reflect the interaction of several processes and that it is commonly difficult to determine their underling cause and hence if they represent daily, monthly or annual time spans (Park, 1976).

In other recent tufa-depositing fluvial environments, porous and dense laminae consisting of cyanobacterial tubes have been attributed to seasonal changes in climate parameters like temperature and temperature-dependent factors such as SIc and microbial growth. This has been based largely on the notion that each laminae couplet represents a year (e.g. Kano et al., 2003, 2007; Andrews & Brasier, 2005; Kawai et al., 2009; Arp et al., 2010). Seasonal sampling allowed Arp et al. (2001) to demonstrate that dense-microcrystalline laminae formed in summer-autumn months, whereas the porous-microspar laminae formed in winter-spring months. Therefore, each dense-porous couplet was interpreted to represent a one-year deposit with the constituent laminae attributed to seasonal changes in temperature and insolation. In many cases, it is not clear in these studies if the laminae are simple or composite as in the case of the River Piedra examples. In Kawai et al. (2009, their Fig. 1), for example, some of the laminae appear to be composite in nature. Gradziński (2010), based on recent tufas in Poland and Slovakia, concluded that they were not characterized by clearly defined seasonal sequences of laminae. In some of these examples, up to 60 laminae formed over a period of 14 months.

Study of the River Piedra stromatolites has demonstrated that laminae development is complex and generally consists of several orders of cyclicity, ranging from seasonal to monthly and perhaps even shorter time spans. Fabrics found in other stromatolites have been attributed to diurnal changes in light that trigger changes in filament orientation (i.e. of *Phormidium hendersonii*) and generates daily or nyctohemeral lamination (Monty, 1965, 1978; Golubić & Focke, 1978; Wright & Wright, 1985; Seong-Joo et al., 2000) that is similar to the microlamination found in the stromatolites from the River Piedra. Okumura et al. (2013), however, argued that the daily laminae evident in some travertine stromatolites can be explained by the diurnal development of the cyanobacterial mat and its inhibiting effect on mineral precipitation through Ca binding ability of EPS. Microlamination consisting of superposed micritic films has been reported from the micritic laminae associated with micritic and microsparitic lamina couplets in Palaeogene stromatolites from the eastern Ebro Basin (Zamarreño et al., 1997).

The formation of several laminae in a few months seems to be common in fluvial carbonate environments with high deposition rates (Ordóñez et al., 1980; Drysdale & Gillieson, 1997; Gradziński, 2010; Manzo et al., 2012). Moreover, several orders of lamination can occur, reflecting both periodic (daily, seasonal, pluriseasonal) and non periodic processes (with a duration range of several months, monthly and weekly). Without the temporal control of the studied tufa stromatolite records in this work, the temporal duration of the different ranks of lamination would have been overestimated.

In many ancient stromatolites and oncolites, the alternating dense and porous laminae have been attributed to variations in temperature, precipitation and/or evaporation (Casanova, 1994; Lindqvist, 1994; Woo et al., 2004; Arenas et al., 2007). In most cases, the duration of such changes is unknown, and a probable duration is generally proposed based on various textural and geochemical considerations (Seong-Joo et al., 2000; Riding, 2000; Arenas et al., 2015). For Holocene lacustrine stromatolites in the East African Rift Valley, for example, Casanova (1994) proposed that each light sparitic lamina and dark micritic lamina couplet represented the ecological cycle of the microbial mat as it responded to seasonal contrast. Accordingly, the light laminae were allied with the rainy seasons, whereas the dark laminae were considered indicative of the dry seasons.

Lindqvist (1994) noted several orders of cyclicity in laminae, based on texture and thickness, in Cretaceous lacustrine oncolites from New Zealand. He suggested that seasonal fluctuations in temperature and light intensity produced couplets 50 to 500 μm thick, but noted that thicker groups of such laminae (~ 1.5 mm thick) probably represented longer climate-induced changes in lake level and nutrient supply.

For Palaeocene to Eocene non-marine stromatolites in the Ebro Basin, the isotopic compositions of the alternating dark and light laminae did not reflect seasonal changes (Zamarreño et al., 1997). The study concluded that the lack of correspondence between textural and isotopic changes ($\delta^{18}O$) reflected the fact that the seasonal contrasts in temperature between the rainy and dry seasons that existed in the eastern Ebro Basin during the Palaeogene were only minor. In contrast, Arenas et al. (2015), based on textural and stable isotope values, tentatively proposed a seasonal to pluriannual duration of the dark and light composite laminae found in oncolites that developed in a Jurassic fluvial rift basin in northern Spain. Using stable isotopes, Brasier et al. (2010) developed evidence for the seasonal origin of the laminae in Pleistocene (~100 ka old) tufas from central Greece. Abrupt changes in $\delta^{18}O$-derived water temperature coupled with sharp textural changes pointed to each laminae couplet (dense and porous laminae, 6 mm thick) being an incomplete record of annual tufa formation.

High resolution ^{14}C dating of a Holocene lacustrine stromatolite from Walker Lake showed that laminae couplets (dense and porous laminae) represented different periodicities from the base to the top of the structure. The most common periodicity was four to six years, which was linked to variations in Ca supply to the lake that were, in turn, related to the climate variability of the region that was probably driven by El Niño Southern Oscillation cycles (Petryshyn et al., 2012). Periodicity analyses of lamina couplet thickness variations and geochemical series in carbonate biolaminites from the early Mesoproterozoic Wumishan Formation (ca.1.5 to 1.45 Ga) of North China led Tang et al. (2014) to deduce solar cycles (11- and 22-year cycles), assuming each light/dark lamina couplet had seasonal origin and represented a year. The latitude inferred for the North China platform (10°N and 25°N) during the Mesoproterozoic supports a dominant arid to semi-arid climate with seasonal changes in temperature. They considered microbial growth rate and biomass production in a subtidal environment were influenced by solar induced climate changes.

Collectively, it is readily apparent that the time duration for the porous and dense lamina couplets ranges from annual (Casanova, 1994; Andrews & Brasier, 2005; Kremer et al., 2008; Brasier et al., 2010; Tang et al., 2014) to pluriannual (Petryshyn et al., 2012). In the River Piedra they can also be formed over shorter time spans. The study of the River Piedra demonstrates that stromatolite lamination is complex and generally involves several orders of cyclicity that can form during a single year. The results of the present study may then help revise the temporal significance of lamination in ancient stromatolites and oncolites of different environments.

CONCLUSIONS

Textural and structural attributes of modern fast-accreting calcite stromatolites that grew in the River Piedra (NE Spain) are characterized by various scales and types of laminae. Correlation of those laminae with the environmental parameters of the area has led to the following important conclusions:

- The stromatolites are formed of dense and porous composite laminae and minor macrocrystalline composite laminae. The former two, mainly alternating through time, consists of micrite and microspar that largely formed from cyanobacteria calcification. The dense composite laminae, up to 15 mm thick, consist of successive dense laminae and/or alternating dense and thinner porous laminae. The porous composite laminae, up to 12 mm thick, consist mainly of porous laminae that can alternate with thinner dense laminae. Each composite lamina is composed of two to eight laminae and represents a few months up to six months, and in some cases a period slightly longer than six months. Microlamination in some composite laminae may have daily duration.
- Macrocrystalline laminae, consisting of crystals > 100 µm long, occur isolated or grouped into composite laminae, most commonly at the base of the warm and cool period deposits and on erosional surfaces. The occurrence of these primary precipitates is linked to the lack of microbial mats during weeks to a few months, either by natural or methodological causes.
- Most boundaries between the deposits formed during warm (spring + summer seasons) and cool (autumn + winter seasons) periods coincide or are very close to the boundaries between composite laminae.
- Alternating dense (thicker) and porous (thinner) composite laminae correlate best with periodic changes in temperature, i.e. seasonal high and low temperature periods,

respectively, and parallel changes in the calcite saturation index. The development of either porous or dense laminae is linked to shorter (e.g., intraseasonal variations) variations in temperature, insolation and/or hydrological conditions.

- Thus, stromatolite lamination can record different-order, periodic and non-periodic changes in magnitude of varied environmental, principally climatic, parameters, ranging from seasonal to monthly and even shorter time spans. These changes affect the cyanobacterial growth and the calcite saturation index.
- These results are relevant to interpreting the processes reflected in other microbial laminated structures, irrespective of their age and depositional environment.

ACKNOWLEDGEMENTS

This study was funded by projects REN2002-03575/CLI, CGL2006-05063/BTE, CGL2009-09216/CLI and CGL2013-42867 of the Spanish Government and European Regional Funds. This work fits the objectives of the “Continental Sedimentary Basins Analysis” research group (Aragón Government and University of Zaragoza, and European Regional Funds). We thank the personnel of the *Servicio de Preparación de Rocas y Materiales Duros* and Scanning Electron Microscopy (*Servicio General de Apoyo a la Investigación-SAI*) of the University of Zaragoza, as well as technicians in the Scanning Electron Microscopy Laboratory of the Department of Earth and Atmospheric Sciences at the University of Alberta for their help. We are grateful to the management and staff of the Monasterio de Piedra Natural Park for facilitating our fieldwork. Our gratitude to L. Auqué, C. Osácar, G. Pardo, C. Sancho and M. Vázquez-Urbez for their collaboration in field and laboratory work, and comments on an earlier version of the manuscript. Comments and suggestions on the manuscript by reviewer G. Della Porta, two anonymous reviewers and associate editor C. Hollis are gratefully acknowledged.

REFERENCES

Andrews, J.E. and **Brasier, A.T.** (2005) Seasonal records of climate change in annually laminated tufas: short review and future prospects. *J. Quatern. Sci.*, **20**, 411–421.

Arenas, C., **Cabrera, L.** and **Ramos, E.** (2007) Sedimentology of tufa facies and continental microbialites from the Palaeogene of Mallorca Island (Spain). *Sed. Geol.*, **197**, 1–27.

Arenas, C., **Vázquez-Urbez, M.**, **Auqué, L.**, **Sancho, C.**, **Osácar, C.** and **Pardo, G.** (2014) Intrinsic and extrinsic controls of spatial and temporal variations in modern fluvial tufa sedimentation: a thirteen-year record from a semi-arid environment. *Sedimentology*, **61**, 90–132.

Arenas, C., **Piñuela, L.** and **García-Ramos, J.C.** (2015) Climatic and tectonic controls on carbonate deposition in syn-rift siliciclastic fluvial systems: a case of microbialites and associated facies in the Late Jurassic. *Sedimentology*, **62**, 1149-1183.

Arp, G., **Wedemeyer, N.** and **Reitner, J.** (2001) Fluvial tufa formation in a hard-water creek (Deinschwanger Bach, Franconian Alb, Germany). *Facies*, **44**, 1–22.

Arp, G., **Bissett, A.**, **Brinkmann, N.**, **Cousin, S.**, **deBeer, D.**, **Friedl, T.**, **Mohr, K.I.**, **Neu, T.R.**, **Reimer, A.**, **Shiraishi, F**., **Stackebrandt, E.** and **Zippel, B.** (2010) Tufa-forming biofilms of German karstwater streams: microorganisms, exopolymers, hydrochemistry and calcification. In: *Tufas and Speleothems: Unravelling the Microbial and Physical Controls* (Eds H.M. Pedley and M. Rogerson), *Geol. Soc. London Spec. Publ*., **336**, 83–118.

Auqué, L., **Arenas, C.**, **Osácar, C.**, **Pardo, G.**, **Sancho, C.** and **Vázquez-Urbez, M.** (2014) Current tufa sedimentation in a changing-slope valley: the River Añamaza (Iberian Range, NE Spain). *Sed. Geol.*, **303**, 26–48.

Berrendero, E., **Arenas, C.**, **Mateo, P.** and **Jones, B.** (2016) Cyanobacterial diversity and related sedimentary facies as a function of water flow conditions: example from the Monasterio de Piedra Natural Park (Spain). *Sed. Geol.*, **337**, 12–28.

Brasier, A.T., **Andrews, J.E.**, **Marca-Bell, A.D.** and **Dennis, P.F.** (2010) Depositional continuity of seasonally laminated tufas: implications for $\delta^{18}O$ based palaeotemperatures. *Global Planet. Change*, **71**, 160–167.

Brasier, A.T., **Andrews, J.E.**, and **Kendall, A.C.** (2011) Diagenesis or dire genesis? The origin of columnar spar in tufa stromatolites of central Greece and the role of chironomid larvae. *Sedimentology*, **58**, 1283–1302.

Burne, R.V. and **Moore, L.S.** (1987) Microbialites: organosedimentary deposits of benthic microbial communities. *Palaios*, **2**, 241–254.

Casanova, J. (1994) Stromatolites from the East African Rift: a synopsis. In: *Phanerozoic Stromatolites II* (Eds J. Bertrand-Sarfati and C. Monty), pp. 193–226. Kluwer Academic Publishers, Dordrecht, The Netherlands.

Chen, J., **Zhang, D.D.**, **Wang, S.**, **Xiao, T.** and **Huang, R.** (2004) Factors controlling tufa deposition in natural waters at waterfall sites. *Sed. Geol.*, **166**, 353–366.

Decho, A.W. (2010) Overview of biopolymer-induced mineralization: what goes on in biofilms? *Ecol. Engineering*, **36**, 137–144.

Drysdale, R.N. and **Gillieson, D.** (1997) Micro-erosion meter measurements of travertine deposition rates: a case study from Louie Creek, northwest Queensland, Australia. *Earth Surf. Proc. Land.*, **22**, 1037–1051.

Dupraz, C. and **Visscher, P.T.** (2005) Microbial lithification in marine stromatolites and hypersaline mats. *Trends in Microbiology*, **13**, 429–438.

Dupraz, C., **Reid, R.P.**, **Braissant, O.**, **Decho, A.W.**, **Norman, R.S.** and **Visscher, P.T.** (2009) Processes of carbonate precipitation in modern microbial mats. *Earth-Sci. Rev.*, **96**, 141-162.

Gebelein, C.D. (1969) Distribution, morphology, and accretion rate of Recent subtidal algal stromatolites, Bermuda. *J. Sed. Petrol.*, **39**, 49-69.

Golubić, S. and **Focke, J.W.** (1978) *Phormidium hendersonii* Howe: identity and significance of a modern stromatolite building microorganism. *J. Sed. Petrol.*, **48**, 751-764.

Golubić, S., **Violante, C.**, **Plenković–Moraj, A.** and **Grgasović, T.** (2008) Travertines and calcareous tufa deposits: an insight into diagenesis. *Geol. Croat.*, ***61***, 363–378.

Gradziński, M. (2010) Factors controlling growth of modern tufa: results of a field experiment. In: *Tufas and Speleothems: Unravelling the Microbial and Physical Controls* (Eds M. Pedley and M. Rogerson), *Geol. Soc. London Spec. Publ.*, **336**, 143–191.

Hofmann, H.J. (1973). Stromatolites: characteristics and utility. *Earth-Sci. Rev.*, **9**, 339-373.

Ihlenfeld, C., **Norman, M.D.**, **Gagan, M.K.**, **Drysdale, R.N.**, **Maas, R.** and **Webb, J.** (2003) Climatic significance of seasonal trace element and stable isotope variations in a modern freshwater tufa. *Geochim. Cosmochim. Acta*, **67**, 2341–2357.

Jiménez-López, C., **Ben Chekroun, K.**, **Jroundi, F.**, **Rodríguez-Gallego, M.**, **Arias, J.M.** and **González-Muñoz, M.T.** (2011) *Myxococcus xanthus* colony calcification: a study to better understand the processes involved in the formation of this stromatolite-like structure. In: *Advances in Stromatolite Geobiology. Lecture Notes in Earth Sciences* (Eds. J. Reitner, N.V. Quéric and G. Arp), pp. 161–181. Springer-Verlag, Berlin.

Jones, B. and **Peng, X.** (2014) Multiphase calcification associated with the atmophytic cyanobacterium *Scytonema julianum*. *Sed. Geol.*, **313**, 91–104.

Jones, B. and **Renaut, W.R.** (1994) Crystal fabrics and microbiota in large pisoliths from Laguna Pastos Grandes, Bolivia. *Sedimentology*, **41**, 1171-1202.

Kano, A., **Matsuoka, J.**, **Kojo, T.** and **Fujii, H.** (2003) Origin of annual laminations in tufa deposits, southwest Japan. *Palaeogeogr. Palaeoclimatol. Palaeoecol.*, **191**, 243–262.

Kano, A., **Kawai, T.**, **Matsuoka, J.** and **Ihara, T.** (2004) High-resolution records of rainfall events from clay bands in tufa. *Geology*, **32**, 793–796.

Kano, A., **Hagiwara, R.**, **Kawai, T.**, **Hori, M.** and **Matsuoka, J.** (2007) Climatic conditions and hydrological change recorded in a high-resolution stable-isotope profile of a recent laminated tufa on a subtropical island, southern Japan. *J. Sed. Res.*, **77**, 59–67.

Kawaguchi, T. and **Decho, A. W.** (2002) Isolation and biochemical characterization of extracellular polymeric secretions (EPS) from modern marine stromatolites and its inhibitory effect on $CaCO_3$ precipitation. *Preparative Biochemistry Biotechnology*, **32**, 51–63.

Kawai, T., **Kano, A.** and **Hori, M.** (2009) Geochemical and hydrological controls on biannual lamination of tufa deposits. *Sed. Geol.*, **213**, 41–50.

Kremer, B., **Kazmierczak, J**. and **Stal, L.J.** (2008) Calcium carbonate precipitation in cyanobacterial mats from sandy tidal flats of the North Sea. *Geobiology*, **6**, 46-46.

Krumbein, W.E., **Brehm, U.**, **Gerdes, G.**, **Gorbushina, A.A.** and **Levit, G.** (2003) Biofilm, biodictyon and biomat – biolaminites, oolites, stromatolites – geophysiology, global mechanism, parahistology. In: *Fossil and Recent Biofilms* (Eds W.E. Krumbein, D.M. Paterson and G.A. Zavarzin), pp. 1–27. Kluwer, Dordrecht.

Lindqvist, J.K. (1994). Lacustrine stromatolites and oncoids. Manuherikia Group (Miocene), New Zealand. In: *Phanerozoic Stromatolites II* (Eds J. Bertrand-Sarfati and C. Monty), pp. 227–254. Kluwer Academic Publishers, Dordrecht, The Netherlands.

Manzo, E., **Perri, E.** and **Tucker, M.E.** (2012) Carbonate deposition in a fluvial tufa system:

processes and products (Corvino Valley – southern Italy). *Sedimentology*, **59**, 553–577.

Matsuoka, J., **Kano, A.**, **Oba, T.**, **Watanabe, T.**, **Sakai, S.** and **Seto, K.** (2001) Seasonal variation of stable isotopic compositions recorded in a laminated tufa, SW Japan. *Earth Planet. Sci. Lett.*, **192**, 31–44.

Meldrum, F. and **Cölfen, H.** (2008) Controlling mineral morphologies and structures in biological and synthetic systems. *Chem. Rev.*, **108**, 4332–4432.

Merz-Preiß, M. and **Riding, R.** (1999) Cyanobacterial tufa calcification in two freshwater streams: ambient environment, chemical thresholds and biological processes. *Sed. Geol.*, **126**, 103–124.

Monty, C.L.V. (1965) Recent algal stromatolites in the Windward Lagoon, Andros Island, Bahamas. *Ann. Soc Géol. Belg.*, **88**, 269-276.

Monty, C.L.V. (1976) The origin and development of cryptalgal fabrics. In: *Stromatolites* (Ed. M.R. Walter), *Dev. Sedimentol.*, **20**, 193–249.

Monty, C.L.V. (1978) Scientific reports of the Belgian expedition on the Australian Great Barrier Reefs, 1967. Sedimentology: 2. Monospecific stromatolites from the Great Barrier Reef Tract and their paleontological significance. *Ann. Soc Géol. Belg*., **101**, 163–171.

Neu, T.R. (1996) Significance of bacterial surface-active compounds in interaction of bacteria with interfaces. *Microbiol. Rev.*, **60**, 151–166.

O'Brien, G.R., **Kaufman, D.S.**, **Sharp, W.D.**, **Atudorei, V.**, **Parnell, R.A.** and **Crossey, L.J.** (2006) Oxygen isotope composition of annually banded modern and mid-Holocene travertine and evidence of paleomonsoon floods, Grand Canyon, Arizona, USA. *Quatern. Res.*, **65**, 366–379.

Okumura, T., **Takashima, C.**, **Shiraishi, F.**, **Nishida, S.** and **Kano, A.** (2013) Processes forming daily lamination in a microbe-rich travertine under low flow condition at the Nagano-yu Hot Spring, southwestern Japan. *Geomicrobiol J.*, **30**, 910–927.

Ordóñez, S., **Carballal, R.** and **García del Cura, A.** (1980) Carbonatos biogénicos actuales en la cuenca del río Dulce (provincia de Guadalajara). *Bol. Real. Soc. Esp. Hist. Nat. (Geol.)*, **78**, 303–315.

Osácar, C., **Arenas, C.**, **Auqué, L.**, **Sancho, C.**, **Pardo, G**. and **Vázquez-Urbez, M.** (2016) Discerning the interactions between environmental parameters reflected in $\delta^{13}C$ and $\delta^{18}O$ of recent fluvial tufas: lessons from a Mediterranean climate region. *Sed. Geol.*, **345**, 126-144.

Park, R.K. (1976) A note on the significance of lamination in stromatolites. *Sedimentology*, **23**, 379–393.

Pedley, H.M. (1994) Prokaryote microphyte biofilms and tufas: a sedimentological perspective. *Kaupia*: *Darmstädter Beitrage zur Naturgeschichte*, **4**, 45-60.

Pedley, M. (1992) Freshwater (phytoherm) reefs: the role of biofilms and their bearing on marine reef cementation. *Sed. Geol.*, **79**, 255-274.

Pedley, M. (2014) The morphology and function of thrombolitic calcite precipitating biofilms: a universal model derived from freshwater mesocosm experiments. *Sedimentology*, **61**, 22-40.

Pedley, H.M., **Rogerson, M.** and **Middleton, R.** (2009) Freshwater calcite precipitates from *in vitro* mesocosm flume experiments: a case for biomediation of tufas. *Sedimentology*, **56**, 511–527.

Peng, X. and **Jones, B.** (2013) Patterns of biomediated $CaCO_3$ crystal bushes in hot spring deposits. *Sed. Geol.*, **294**, 105–117.

Pentecost, A. (1975) Calcium Carbonate Deposition and Blue-green Algae. PhD thesis. University of Wales (UK).

Pentecost, A. (2005) *Travertine*. Springer-Verlag, Berlin, 445 p.

Pentecost, A. and **Franke, U.** (2010) Photosynthesis and calcification of the stromatolitic freshwater cyanobacterium *Rivularia*. *European J. Phycol.*, **45**, 345–353.

Petryshyn, V.A., **Corsetti, F.A.**, **Berelson, W.M.**, **Beaumont, W.** and **Lund, S.P.** (2012) Stromatolite lamination frequency, Walker Lake, Nevada: implications for stromatolites as biosignatures. *Geology*, **40**, 499–502.

Plummer, L.N., **Wigley, T.M.L.** and **Parkhurst, D.L.** (1978) The kinetics of calcite dissolution in CO2–water system at 5° to 60 °C and 0.0 to 1.0 atm CO2. *Am. J. Sci.*, **278**, 179–216.

Preiss, W.V. (1972) The Systematics of South Australian Precambrian and Cambrian Stromatolites, Part 1. *South Australia Royal Society, Transactions*, **96**, 67–100.

Reid, R.P., **Visscher, P.T.**, **Decho, A.W.**, **Stolz, J.K.**, **Bebout, B.M.**, **Dupraz, C.**, **Macintyre, I.G.**, **Paerl, H.W.**, **Pinckney, J.L.**, **Prufert-Bebout, L.**, **Steppe, T.F.** and **DesMarais, D.J.** (2000) The role of microbes in accretion, lamination and early lithification of modern marine stromatolites. *Nature*, **406**, 989–992.

Riding, R. (1991) Classification of microbial carbonates. In: *Calcareous Algae and Stromatolites* (Ed. R. Riding), pp. 21–51, Springer-Verlag, Berlin.

Riding, R. (2000) Microbial carbonates: the geological record of calcified bacterial–algal mats and biofilms. *Sedimentology*, **47**, 179–214.

Rogerson, M., **Pedley, H.M.**, **Wadhawan, J.D.** and **Middleton, R.** (2008) New insights into biological influence on the geochemistry of freshwater carbonate deposits. *Geochim. Cosmochim. Acta*, **72**, 4976-4987.

Rogerson, M., **Pedley, H.M.** and **Middleton, R.** (2010) Microbial influence on macroenvironment chemical conditions in alkaline (tufa) streams: perspectives from *in vitro* experiments. In: *Tufas and Speleothems: Unravelling the Microbial and Physical Controls* (Eds H.M. Pedley and M. Rogerson), *Geol. Soc. London Spec. Publ.*, **336**, 65–81.

Rosenberg, E. (1989) Biofilms on water-soluble substrates. In: *Structure and Function of*

Biofilms (Eds W.G. Characklis and P.A. Wilderer), pp. 59–72, Wiley, Chichester, UK.

Sancho, C., **Arenas, C.**, **Vázquez-Urbez, M.**, **Pardo, G.**, **Lozano, M.V.**, **Peña-Monné, J.L.**, **Hellstrom, J.**, **Ortiz, J.E.**, **Osácar, M.C.**, **Auqué, L.** and **Torres, T.** (2015) Climatic implications of the Quaternary fluvial tufa record in the NE Iberian Peninsula over the last 500 ka. *Quatern. Res.*, **84**, 398–414.

Seong-Joo, L., **Browne, K.M.** and **Golubic, S.** (2000) On stromatolite lamination. In: *Microbial Sediments* (Eds R. Riding and S.M. Awramik), pp. 16–24. Springer-Verlag, Berlin.

Servicio Geológico de Obras Públicas (1990) *Estudio de los recursos hidráulicos subterráneos de los acuíferos relacionados con la provincia de Zaragoza. Unidad hidrogeológica nº 43. Sierra del Solorio*. Informe interno, Madrid, 210 pp.

Shiraishi, F., **Reimer, A.**, **Bisset, A.**, **de Beer, D.** and **Arp, G.** (2008) Microbial effects on biofilm calcification, ambient water chemistry and stable isotope records in a highly supersaturated setting (Westerhöfer Bach, Germany). *Palaeogeogr. Palaeoclimatol. Palaeoecol.*, **262**, 91–106.

Spadaphora, A., **Perri, E.**, **Mckenzie, J.A.** and **Vasconcelos, C.** (2010) Microbial biomineralization processes forming modern Ca:Mg carbonate stromatolites. *Sedimentology*, **57**, 27-40.

Stolz, J.F. (2000) Structure of microbial mats and biofilms. In: *Microbial Sediments* (Eds R. Riding and S.M. Awramik), pp. 1–8. Springer-Verlag, Berlin.

Storrie-Lombardi, M.C. and **Awramik, S.M**. (2006) A sideways view of stromatolites: complexity metrics for stromatolite laminae. In: *Instruments, Methods and Missions for Astrobiology IX* (Eds R.B. Hoover, G.V. Levin and A. Y Rozanov), Proc. SPIE, **6309**, 1–12.

Suárez-González, P., **Quijada, I.E.**, **Benito, M.I.**, **Mas, R.**, **Merinero, R.** and **Riding, R.**

(2014) Origin and significance of lamination in Lower Cretaceous stromatolites and proposal for a quantitative approach. *Sed. Geol.*, **300**, 11–27.

Tang, D., **Shi, X.** and **Jiang, G.** (2014) Sunspot cycles recorded in Mesoproterozoic carbonate biolaminites. *Precambrian Res.*, **248**, 1-16.

Vasconcelos, C., **Dittrich, M.** and **McKenzie, J.A.** (2013) Evidence of microbiocoenosis in the formation of laminae in modern stromatolites. *Facies*, **60**, 3–13.

Vázquez-Urbez, M., **Arenas, C.**, **Sancho, C.**, **Osácar, C.**, **Auqué, L.** and **Pardo, G.** (2010) Factors controlling present-day tufa dynamics in the Monaterio de Piedra Natural Park (Iberian Range, Spain): depositional environmental settings, sedimentation rates and hydrochemistry. *Int. J. Earth Sci. (Geol. Rundsch.),* **99**, 1027–1049.

Vázquez-Urbez, M., **Pardo, G.**, **Arenas, C.** and **Sancho, C.** (2011) Fluvial diffluence episodes reflected in the Pleistocene tufa deposits of the River Piedra (Iberian Range, NE Spain). *Geomorphology*, **125**, 1–10.

Vázquez-Urbez, M., **Arenas, C.** and **Pardo, G.** (2012) A sedimentary facies model for stepped, fluvial tufa systems in the Iberian Range (Spain): the Quaternary Piedra and Mesa valleys. *Sedimentology*, **59**, 502–526.

Walter, M. A. (1972) Stromatolites and the biostratigraphy of the Australian Precambrian and Cambrian. *Special Papers in Palaeontology*, **11**, Palaeontological Association London, 190 pp.

Woo, K.S., **Khim, B.K.**, **Yoo, H.S.** and **Lee, K.C.** (2004) Cretaceous lacustrine stromatolites in the Gyeongsang Basin (Korea): records of cyclic change in paleohydrological condition. *Geosci. J.*, **8**, 179–184.

Wright, V.P. and **Wright, J.M.** (1985) A Stromatolite Built by a Phormidium-Like Alga from the Lower Carboniferous of South Wales. In: *Paleoalgology: Contemporary Research and Applications* (Eds D.F. Toomey and M.H. Nitecki), pp. 40-54. Springer-

Verlag, Berlin.

Zamarreño, I., **Anadón, P.** and **Utrilla, R.** (1997) Sedimentology and isotopic composition of Upper Palaeocene to Eocene non-marine stromatolites, eastern Ebro Basin, NE Spain. *Sedimentology*, **44**, 159–176.

FIGURE CAPTIONS

Fig. 1. (A) Geographic location of the study area. (B) Geological map of the study area with location of the studied sites and main springs (S1 and S2) in the River Piedra. (C) Detail of the River Piedra course in the Monasterio de Piedra Natural Park, with location of study sites within the Park (modified from Arenas et al., 2014).

Fig. 2. The concepts of lamina and composite laminae used in this work based on a stromatolite deposit in the River Piedra.

Fig. 3. Field views of depositional environments and tablet cross-sections with stromatolites. (A) to (D) Fast-flowing water areas devoid of macrophytes and correspondent deposits. (B) Plan view of tablet. (C) and (D) Cross-sections of two tablets (consecutive records) installed at the same site (that of image A), with indication of six-month deposit periods. (E) to (H) Stepped waterfall with strong flow zones and corresponding deposits. (F) Plan view of tablet with stromatolite and moss and filamentous algal boundstone. (G) and (H) Cross-sections of two tablets (consecutive records) installed at the same waterfall (that of E), with indication of six-month deposit periods.

Fig. 4. Stromatolite lamination in tablet cross-sections. Differences in porosity, colour shade and crystal size allow to distinguish dense and porous composite laminae and macrocrystalline composite laminae. (A) to (C) Stromatolite formed in fast-flowing water

areas devoid of macrophytes. Note that (A) is a detail of Fig. 3D. (D) Stromatolite formed in strong flow zone in a stepped waterfall. Note that (D) is a detail of Fig. 3G.

Fig. 5. (A) and (B) Images (optical microscope) showing the three types of laminae and composite laminae across deposits recorded on tablets P-14 (A) and P-16 (B). Deposit in (A) spans from April 2004 to September 2006. Deposit in (B) spans from October 2009 to September 2011 (incomplete warm period 2011, see Fig. 4C). Note microlamination in the porous laminae.

Fig. 6. Detailed images (optical microscope and SEM) showing the three types of laminae and composite laminae, with indication of six-month duration in (A), (B) and (F). (A) Dense and macrocrystalline composite laminae, and porous lamina at the top of image, formed in a stepped waterfall. Note the adjacent fan-shaped bodies at the base (arrow). (B) to (H) Stromatolites formed in fast-flowing water areas without macrophytes. (B) Dense and porous composite laminae. Note an erosional surface at the top (dashed line) over which macrocrystals developed mixed with dense lamina. (C) Microlamination in a dense composite laminae. (D) Detail of microlaminae in SEM. Note that tubes are subperpendicular in the microlaminae and that subhorizontal tubes occur at the microlamina boundaries (arrows). (E) Alternating porous and dense laminae in a porous composite laminae. Note microlamination in the porous laminae. (F) Macrocrystalline composite laminae at the base of tablet and at the top of a dense lamina. (G) Dense composite laminae with mouldic porosity from insects. Note the development of large-crystal lenses over the cavities. (H) Detail of macrocrystals at the top of an insect cavitity. Legend for (A), (B), (E) and (F) in Fig. 5.

Fig. 7. SEM images showing structural and textural features of dense and porous laminae. (A) Three successive laminae consisting of fence-like structures made of subperpendicular tubes (Warm 05). Note that the lamina at the base is more porous and the tubes have diverse orientations. (B) Domed structure in a porous laminae (Cool 04-05). Note the radial

disposition of tubes, the microlamination and the decreasing porosity toward the top. (C) Calcite tubes with mostly subperpendicular disposition forming a dense fabric (Warm 09). (D) Calcite tubes with diverse orientation forming a porous fabric (Cool 04-05). (E) Dense fabric consisting of subparallel calcite tubes formed from calcification of *Phormidium incrustatum* cells (Warm 04). (F) Calcite tube formed from calcification around *P. incrustatum* cells and smaller tubes formed from calcification around smaller filamentous cyanobacteria, problably *Leptolyngbya* sp (Warm 04). Note matrix between tubes formed of calcite crystals of diverse size, diatoms and EPS.

Fig. 8. SEM images showing calcification attributes of calcite tubes in the dense and porous laminae. (A) and (B) Calcite walls with increasing crystal size outward. Note rhombohedra in (B). (C) Calcite wall mainly made of nanocrystals and nanoparticles with development of rhombohedra outward (arrow). Note filamentous bacteria (arrow). (D) Thin calcite wall made of nanoparticles. (E) Detail of inner part of calcite wall with rhombohedral mesocrystal. (F) View parallel to calcite tube (outer surface) with diverse crystal shapes. Note large size of mesocrystals. (G) Trigonal crystals on outer surface of tube. EPS is arrowed. (H) and (I) EPS (arrowed) among calcite crystals of diverse shape (rhombohedrom is arrowed). (J) Diatom partially coated with calcite nanoparticles and EPS (arrow).

Fig. 9. SEM images showing lamination, textural features and calcification attributes of calcite tubes (from *P. incrustatum*) in dense (and less common porous) laminae within dense composite laminae formed in warm periods. (A) Successive dense laminae. Note subhorizontal tubes at the boundary between laminae (arrow). (B) Mainly subperpendicular, parallel tubes in a dense lamina. (C) to (E) Calcite encrustations. Note larger crystals outward. (F) Detail of calcite encrustation with nanocrystals and nanoparticles. Note that the sheath is preserved (EPS).

Fig. 10. SEM images showing lamination, textural features and calcification attributes of calcite tubes (from *P. incrustatum*) in porous (and less common dense) laminae within porous composite laminae formed in cool periods. (A) Successive porous laminae separated by thin macrocrystalline laminae. (B) Mainly subperpendicular and oblique, tubes in a porous lamina. (C) to (E) Calcite encrustations. Note larger crystals outward. (F) Detail of calcite encrustation with mesocrystals. Note that the sheath (EPS) encompasses nanoparticles.

Fig. 11. SEM images showing textural features and calcification attributes of macrocrystalline composite laminae and laminae. (A) Macrocrystalline composite lamina consisting of two macrocrystalline laminae. Note cyanobacterial tubes (arrow) between the laminae and among the macrocrystals that formed in relation to resurgence of the cyanobacterial growth. (B) Detail of (A). Note elongate mesocrystals. (C) Detail of mesocrystal made of rhombohedral nanocrystals. Note mesocrystal is structureless in cross-section. (D) Detail of a mesocrystal. Note cavity in the upper part. Fragment of diatom is attached to top. (E) Detail of nanocrystals. (F) Subhorizontal calcite tubes on a macrocrystalline lamina.

Fig. 12. Correlation between (A) texture of stromatolite formed at site P-14 (location in Fig. 1C), (B) hourly and mean monthly water temperature and (C) daily water discharge from October 2009 to September 2012. Daily discharge data from *Confederación Hidrográfica del Ebro* (http://195.55.247.237/saihebro/), available until June 2012.

Fig. 13. Correlation between (A) texture of stromatolite formed at site P-16 (location in Fig. 1C), (B) hourly and mean monthly water temperature and (C) daily water discharge, from October 2009 to September 2012. Daily discharge data from *Confederación Hidrográfica del Ebro* (http://195.55.247.237/saihebro/), available until June 2012.

TABLE CAPTIONS

Table 1. Mean flow velocity, water depth and deposition rates obtained from November 1999 to September 2012 at the study sites with fast-flow and stromatolite formation in the River Piedra (compiled from Arenas et al., 2014). Cool = October to March period. Warm = April to September period. A: Stromatolites. C: Moss and filamentous algal boundstones. Mean water velocity and depth were measured at the end of each season.

Table 2. Mean values of main hydrochemical characters of the studied sites with stromatolites in the River Piedra (compiled from Arenas et al., 2014). Water for hydrochemistry was sampled at the end of June and in December-January. Temperature was measured on site at the time of sampling. A: Stromatolites. C: Moss and filamentous algal boundstones.

Table 3. Main features of the types of laminae and composite laminae in the River Piedra stromatolites.

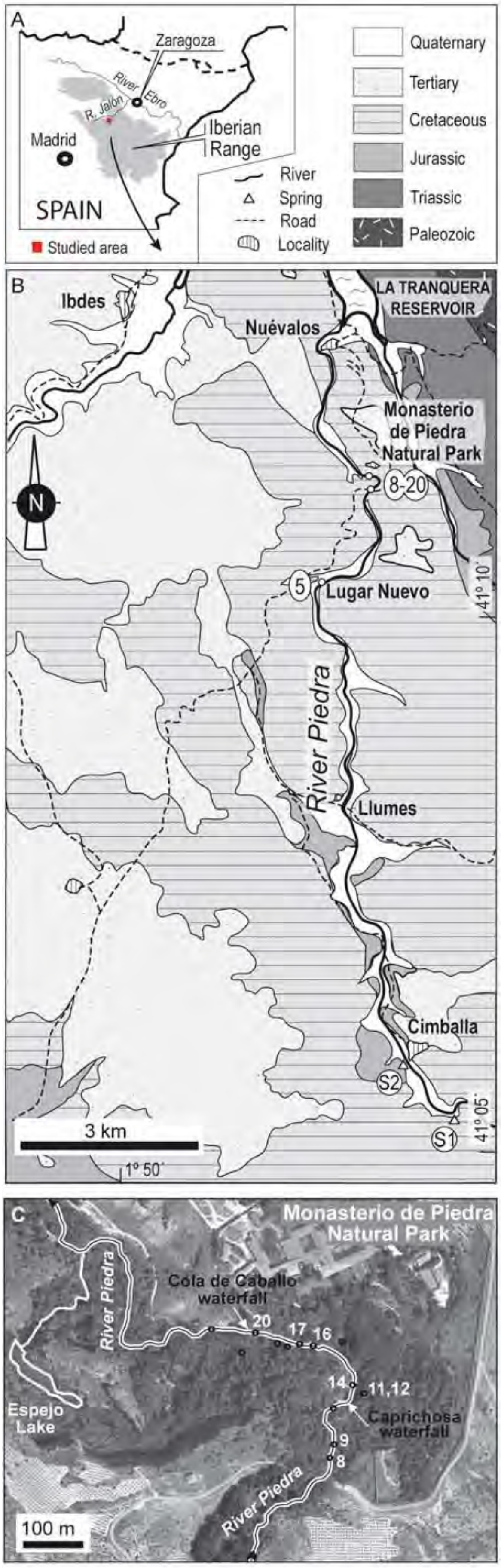

16 Sites with stromatolites studied in this work
Sites for sedimentation and hydrochemistry monitoring

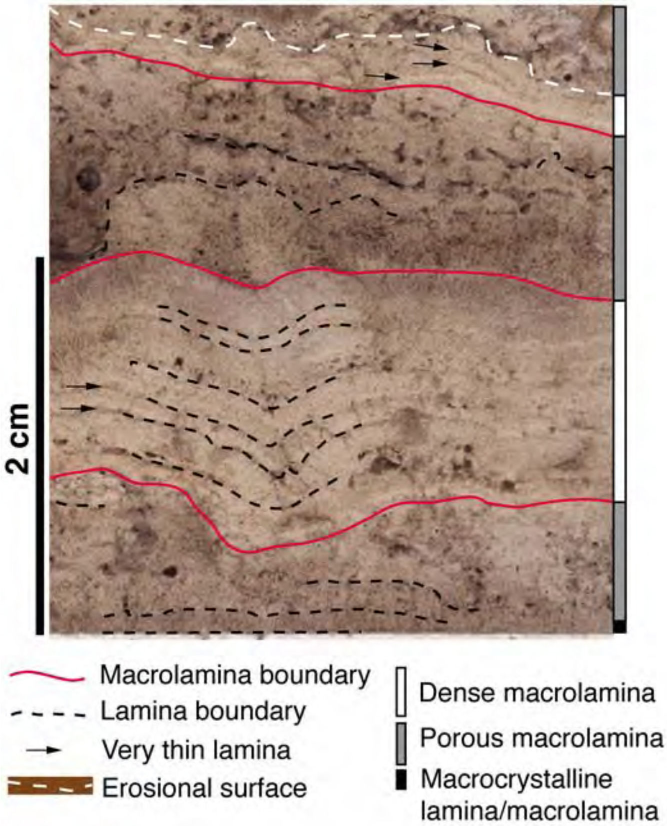
2 cm
Macrolamina boundary
Lamina boundary
Very thin lamina
Erosional surface
Dense macrolamina
Porous macrolamina
Macrocrystalline lamina/macrolamina

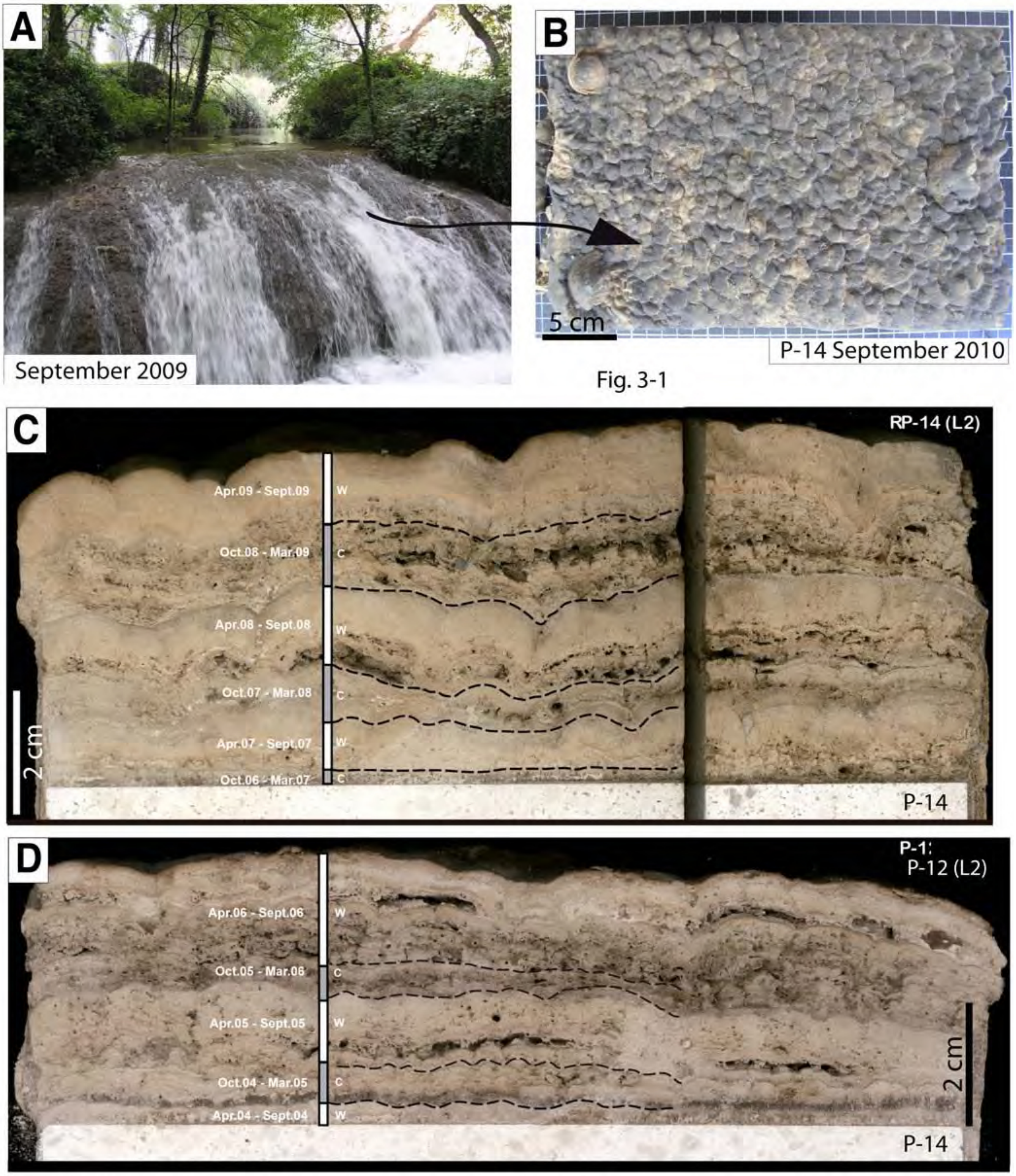

Fig. 3-1

RP-14(L2) and P-12(L2) are the working labels. The tablets were at the same site and will be named P-14 (as in Sedimentology 2014)

Fig. 3-1

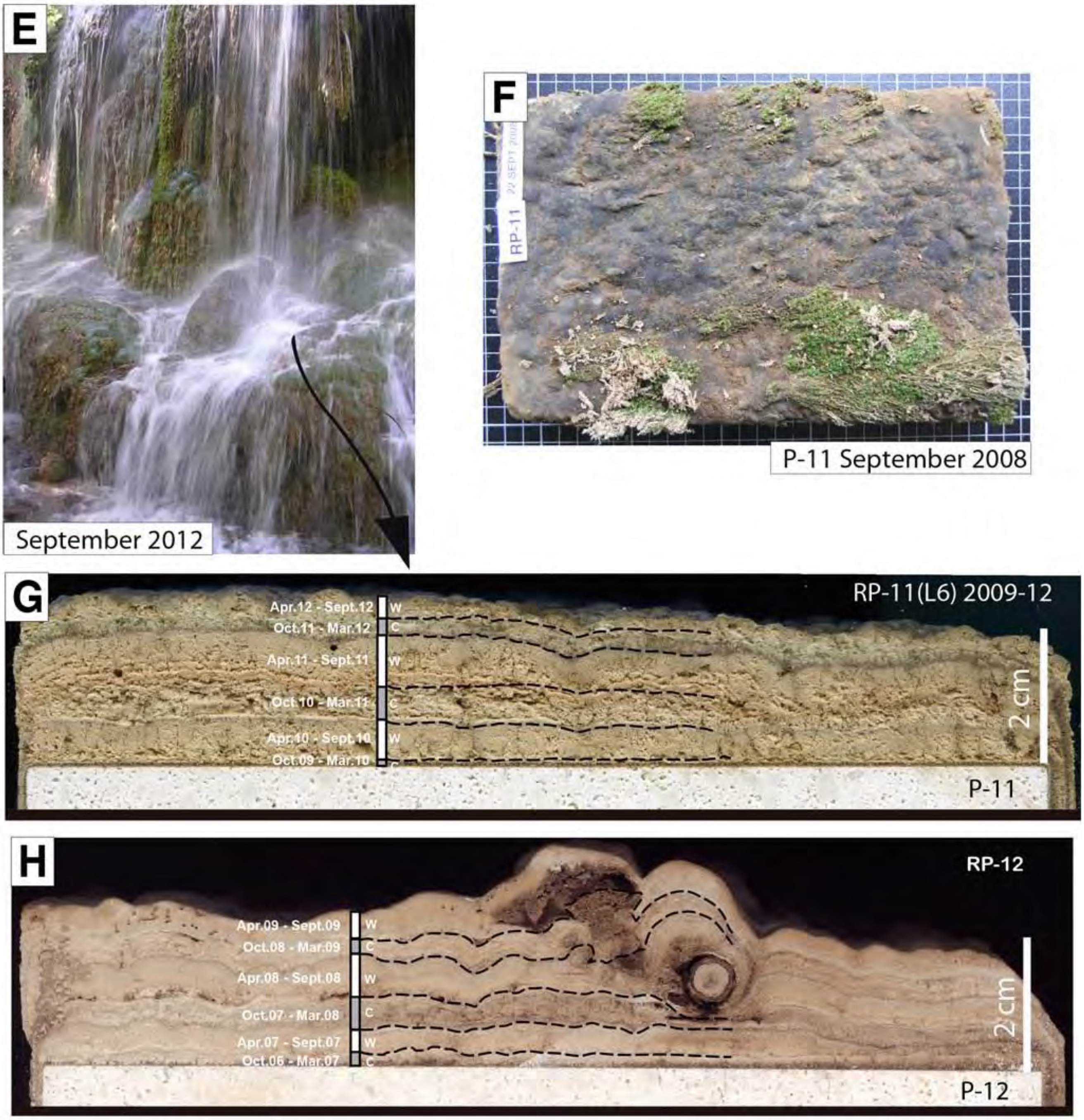

RP-11(L6) and RP-12 are the working labels. The tablets will be named P-11 and P-12 (as in Sedimentology 2014). These two tablets are very close to each other.

Fig. 3-2

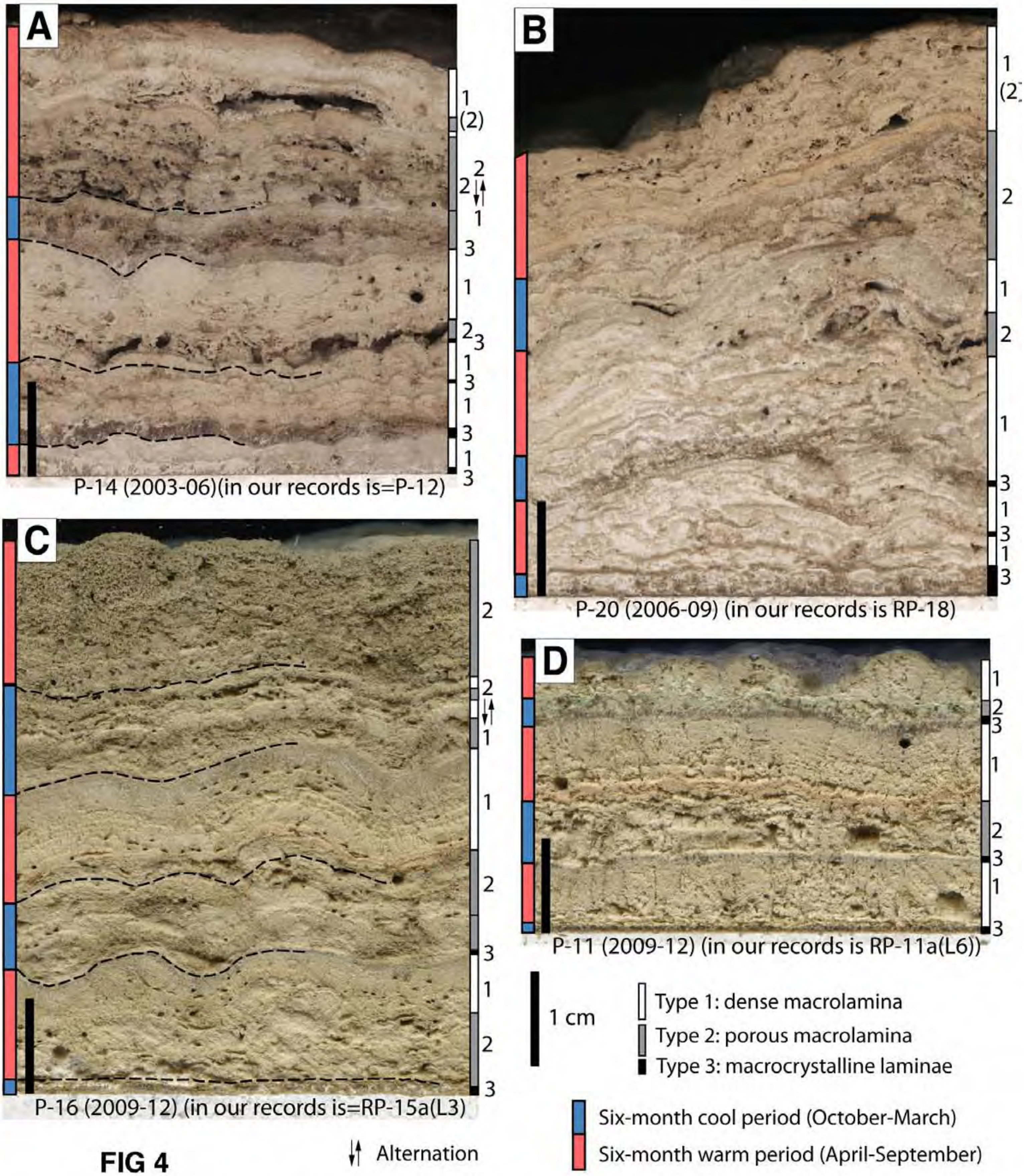

FIG 4

P-16 (2009-12) = that is the label that will appear in the paper (= labels in Sedimentology 2014)

(in our records is=RP-15a(L3)) = that is the label of the several working compaigns, for our reference. That text will be deleted in the final version.

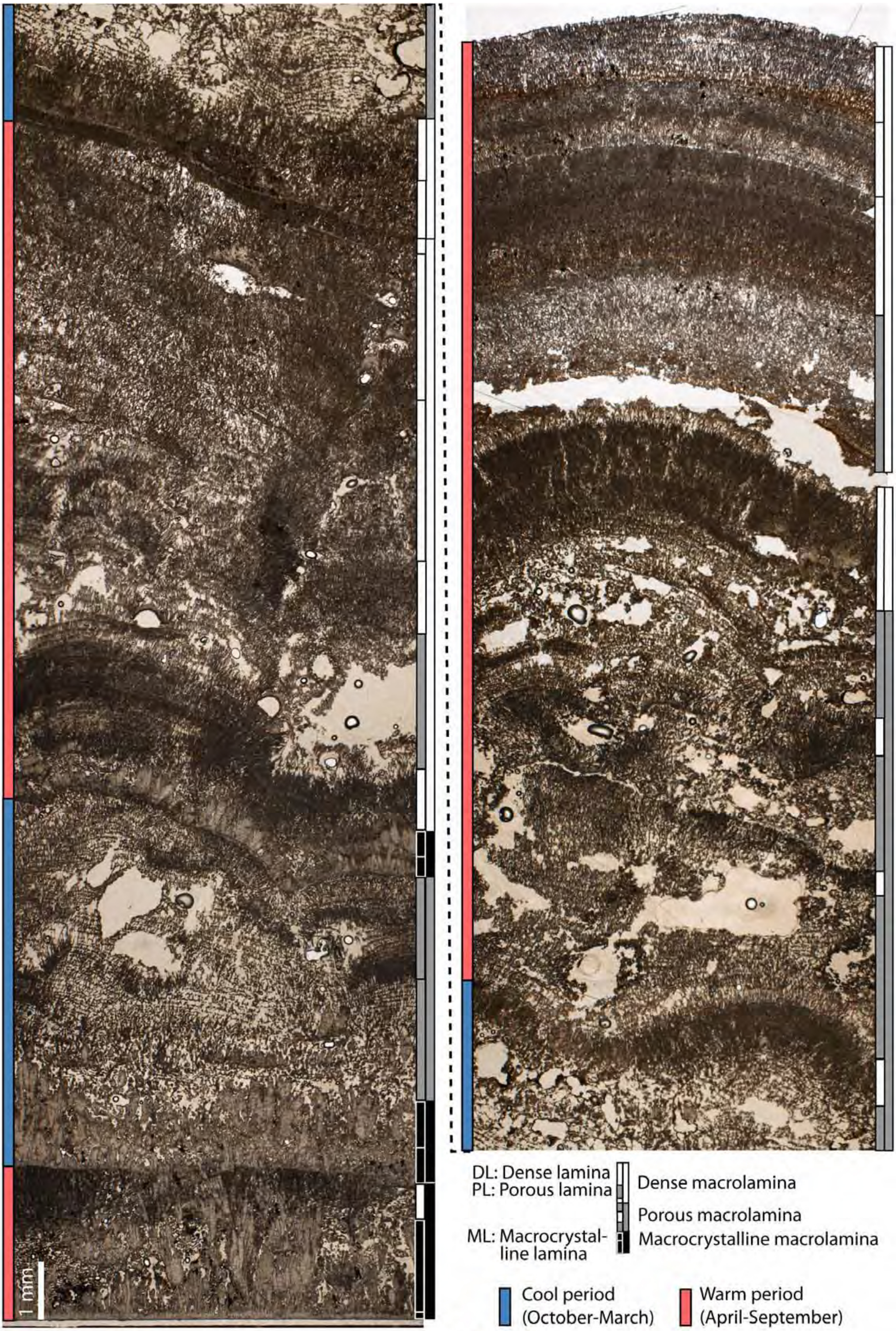

1 mm
DL: Dense lamina
PL: Porous lamina
ML: Macrocrystal-line lamina
Dense macrolamina
Porous macrolamina
Macrocrystalline macrolamina
Cool period (October-March)
Warm period (April-September)

Fig 05-1

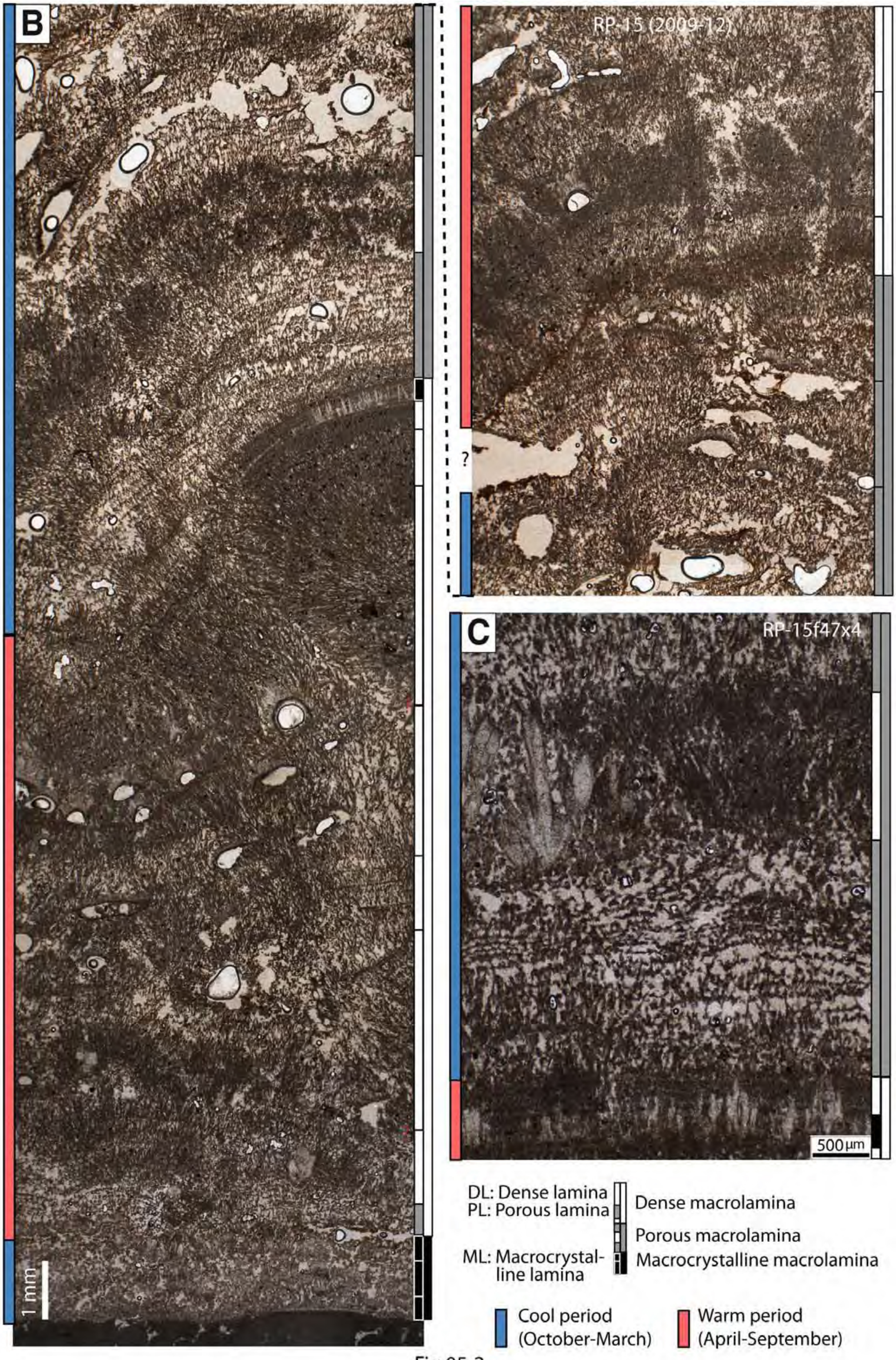
B
1 mm
RP-15 (2009-12)
?
C
RP-15f47x4
500 µm
DL: Dense lamina
PL: Porous lamina
ML: Macrocrystal-line lamina
Dense macrolamina
Porous macrolamina
Macrocrystalline macrolamina
Cool period (October-March)
Warm period (April-September)

Fig 05-2

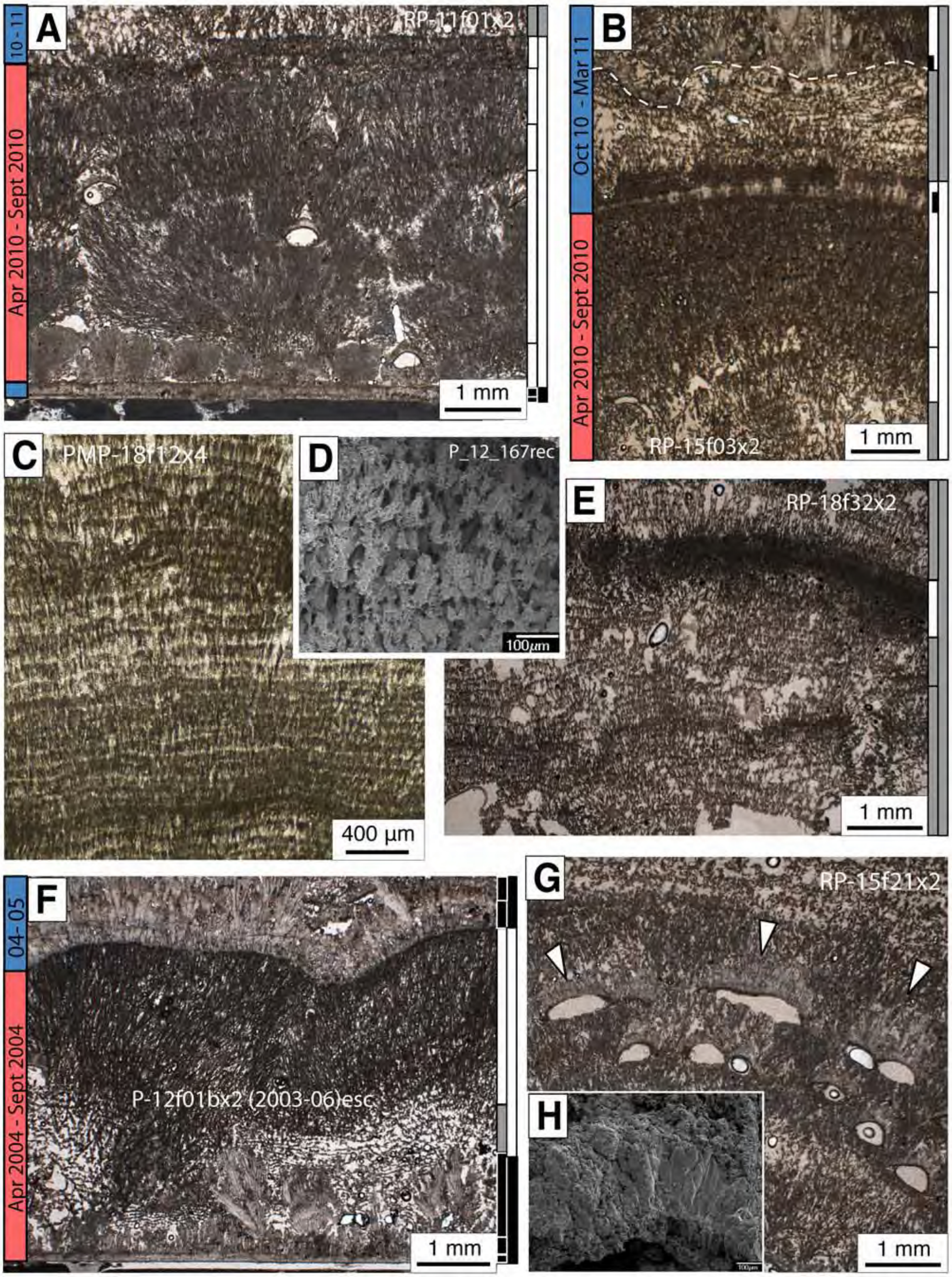

Fig. 6-version B

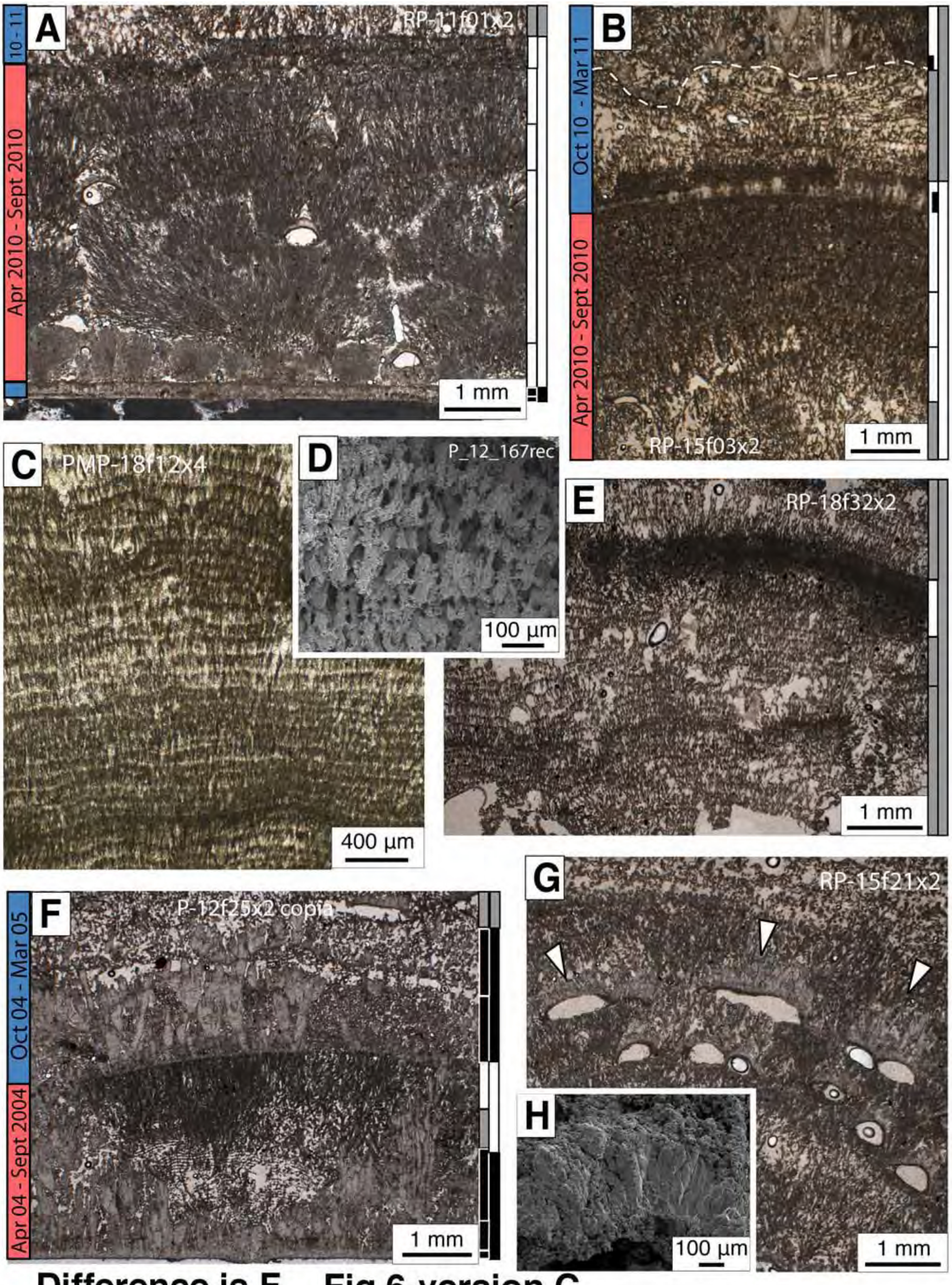

Difference is F **Fig 6-version C**

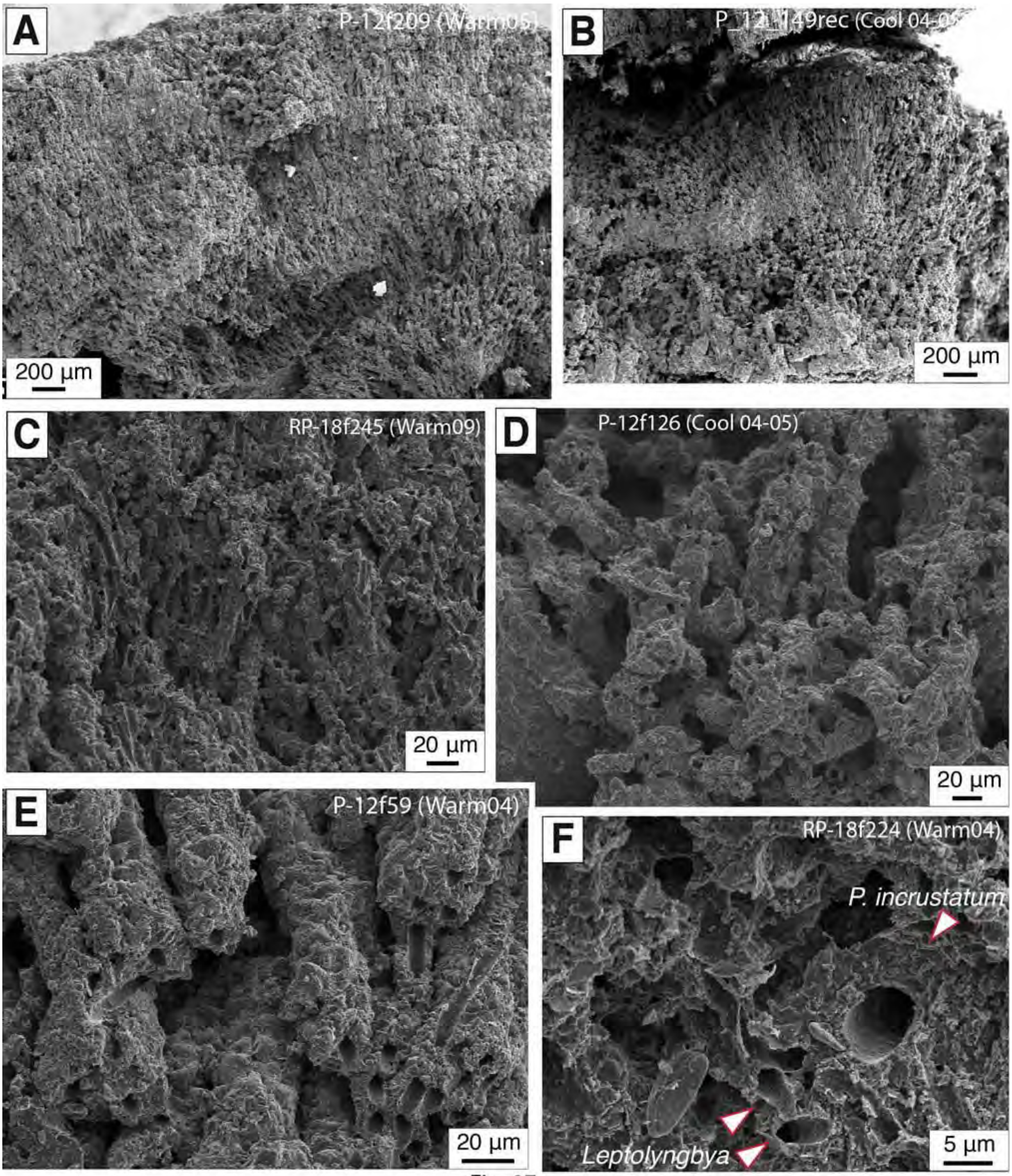
A
P-12f209 (Warm06)
200 µm
B
P_12_149rec (Cool 04-05)
200 µm
C
RP-18f245 (Warm09)
20 µm
D
P-12f126 (Cool 04-05)
20 µm
E
P-12f59 (Warm04)
20 µm
F
RP-18f224 (Warm04)
P. incrustatum
Leptolyngbya
5 µm

Fig. 07

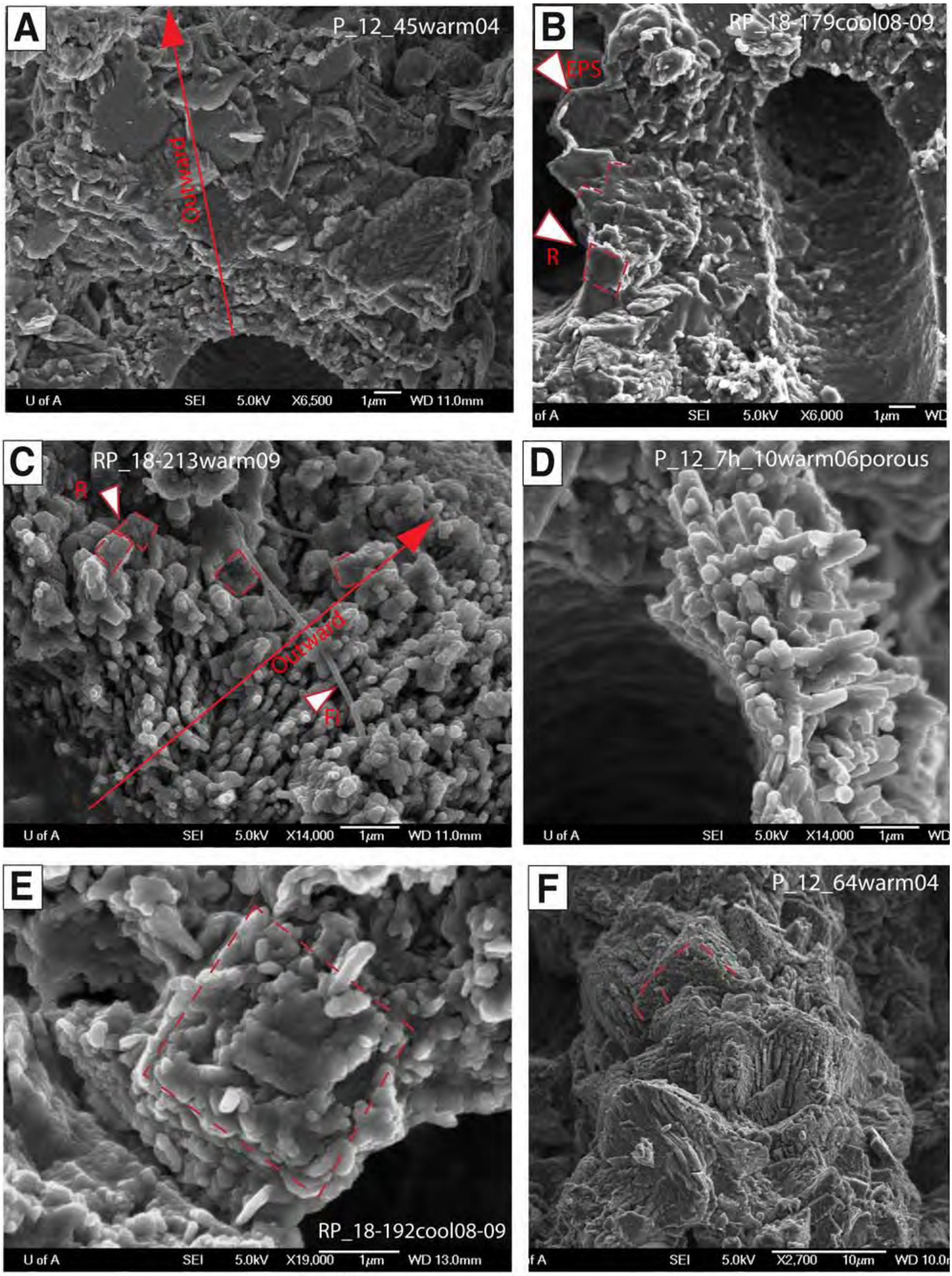

A
P_12_45warm04
Outward
U of A SEI 5.0kV X6,500 1μm WD 11.0mm
B
RP_18-179cool08-09
EPS
R
of A SEI 5.0kV X6,000 1μm WD
C
RP_18-213warm09
R
Outward
Fi
U of A SEI 5.0kV X14,000 1μm WD 11.0mm
D
P_12_7h_10warm06porous
U of A SEI 5.0kV X14,000 1μm WD
E
RP_18-192cool08-09
U of A SEI 5.0kV X19,000 1μm WD 13.0mm
F
P_12_64warm04
f A SEI 5.0kV X2,700 10μm WD 10.0

Fig. 08-1

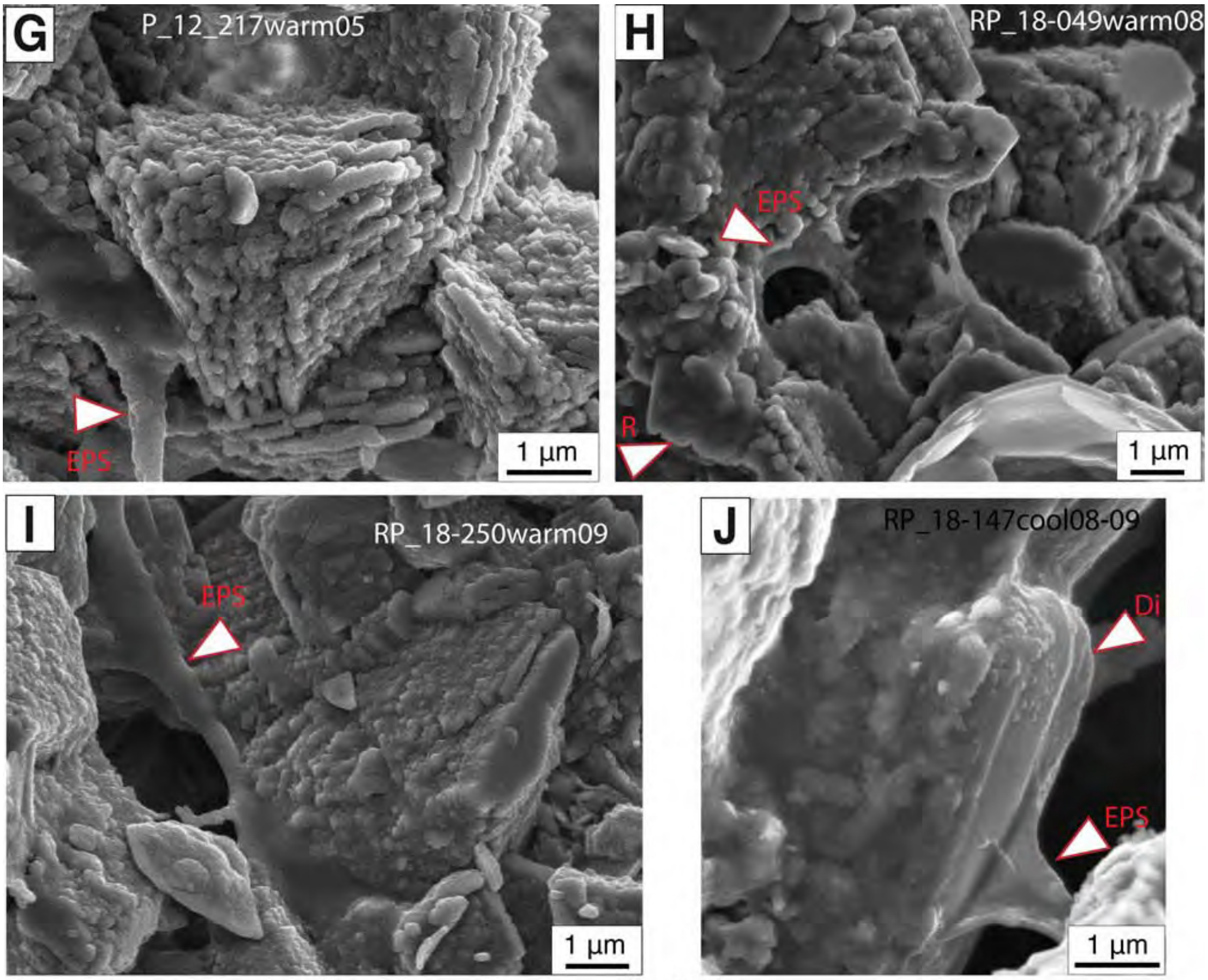
G
P_12_217warm05
EPS
1 µm
H
RP_18-049warm08
EPS
R
1 µm
I
RP_18-250warm09
EPS
1 µm
J
RP_18-147cool08-09
Di
EPS
1 µm

Fig. 08-2

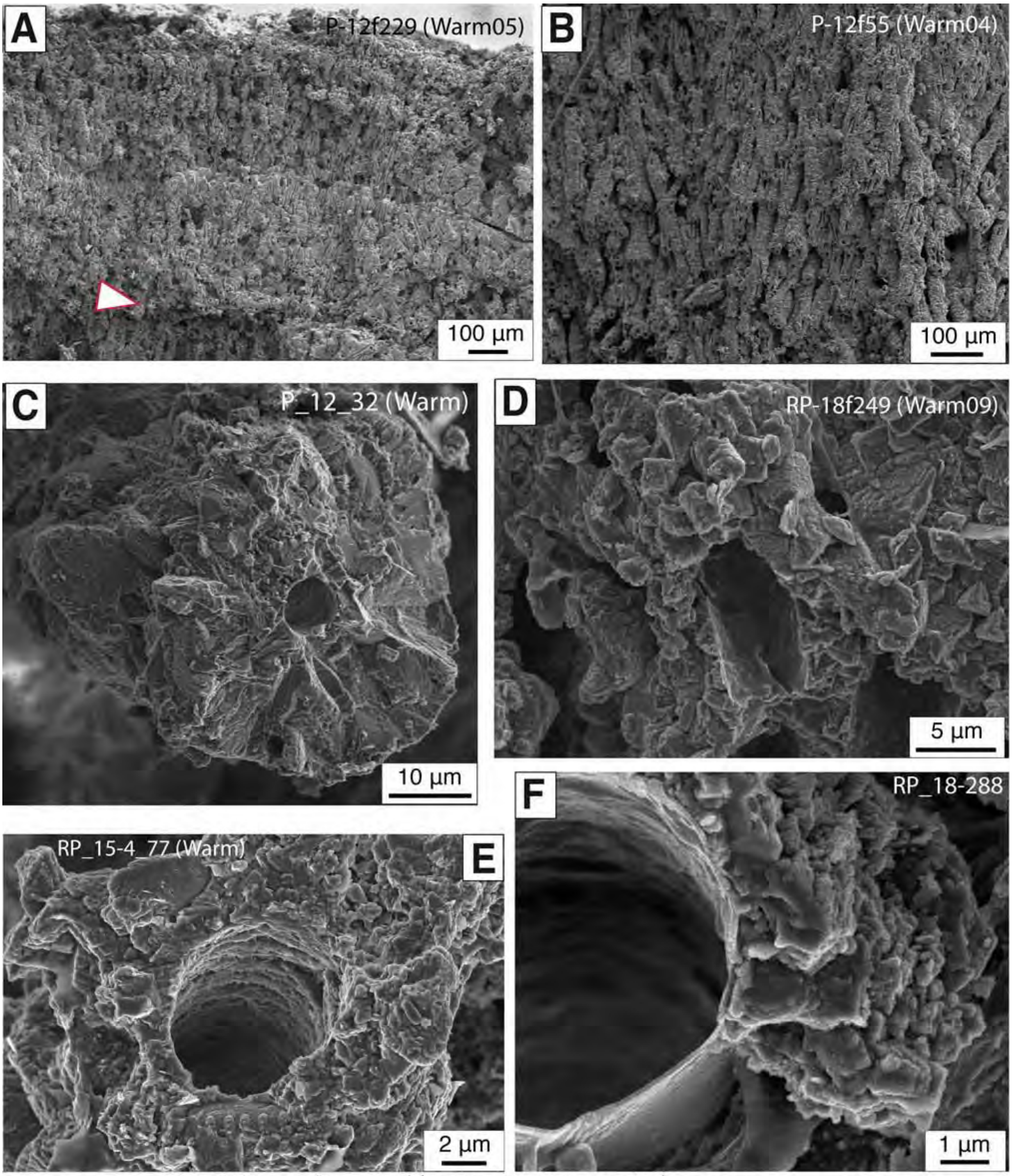

Fig. 09-Dense (+porous) laminae in warm periods

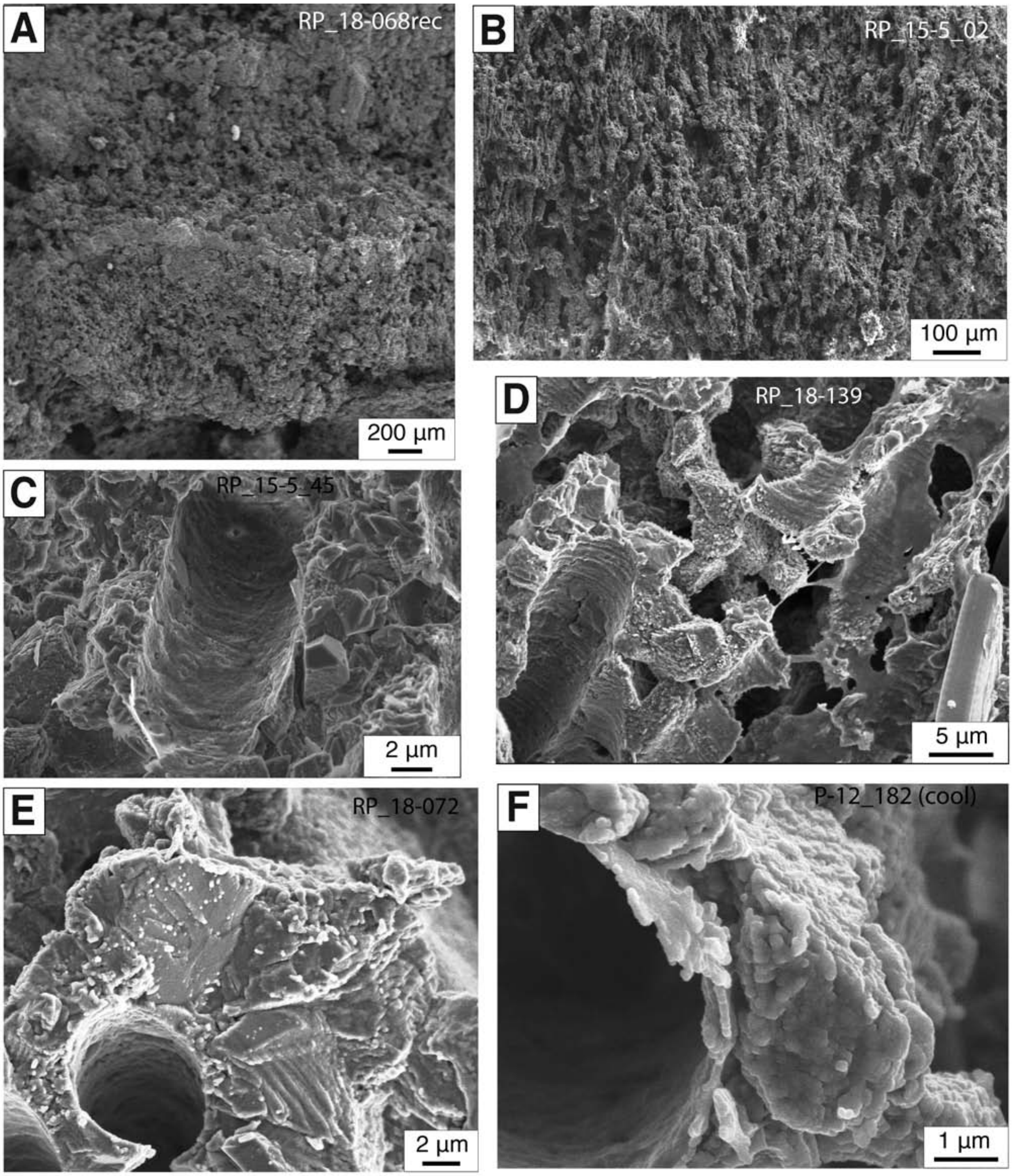

Fig.**10** -Porous (+dense) laminae in cool periods

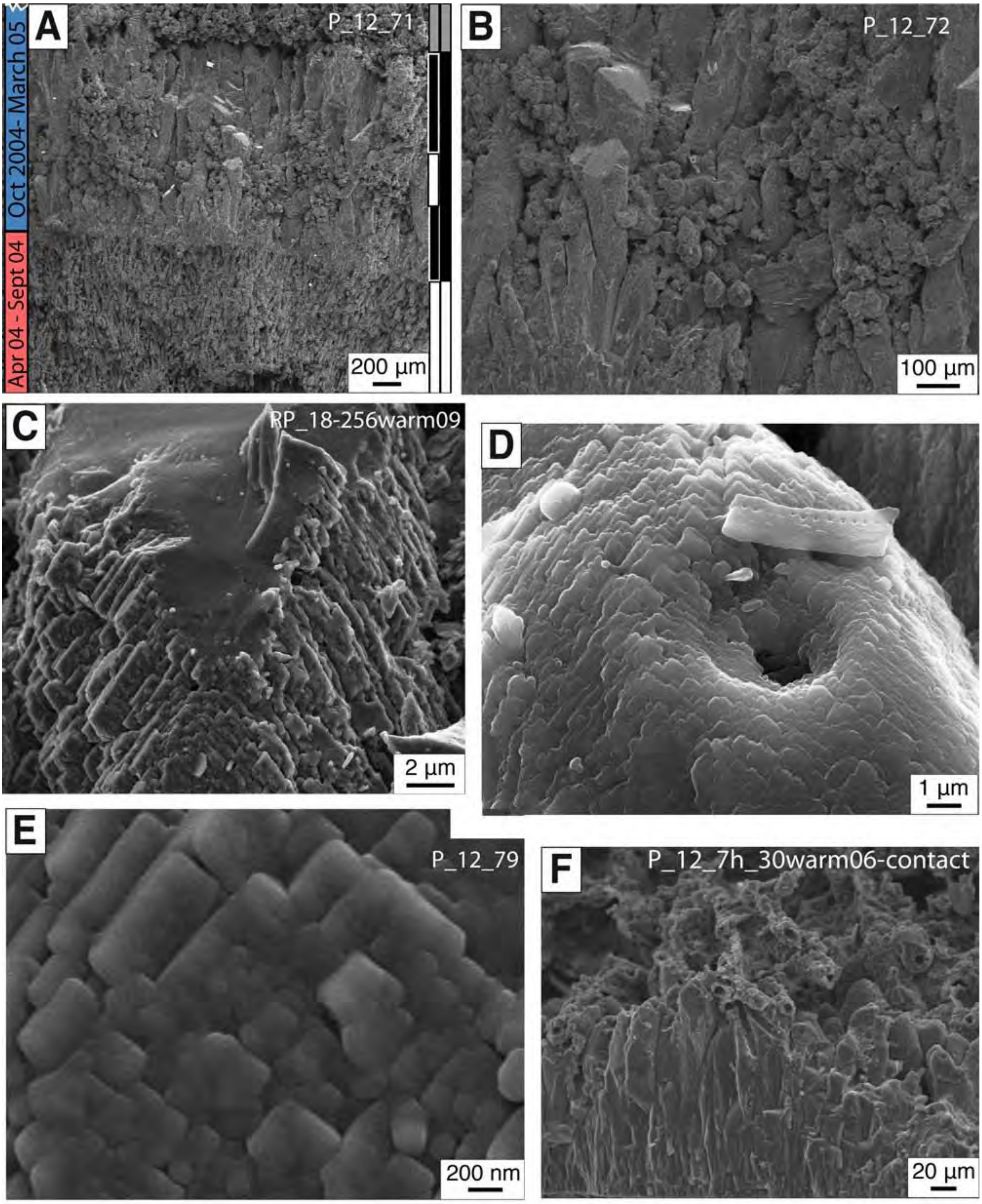

Fig 11-Macrocrystalline

FIG 12-1. PRELIMINARY CORRELATION.

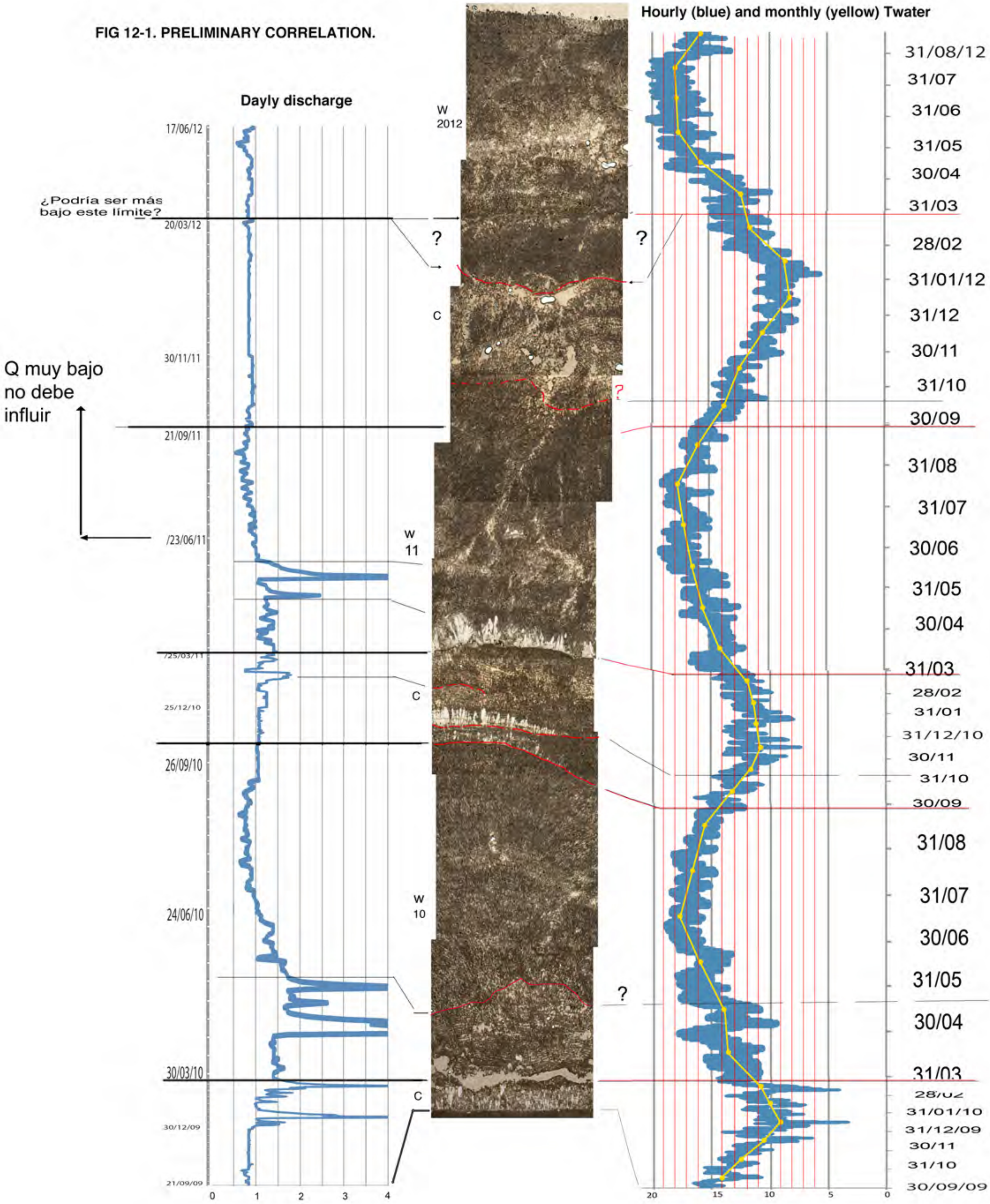

FIG 12-2 PRELIMINARY CORRELATION.

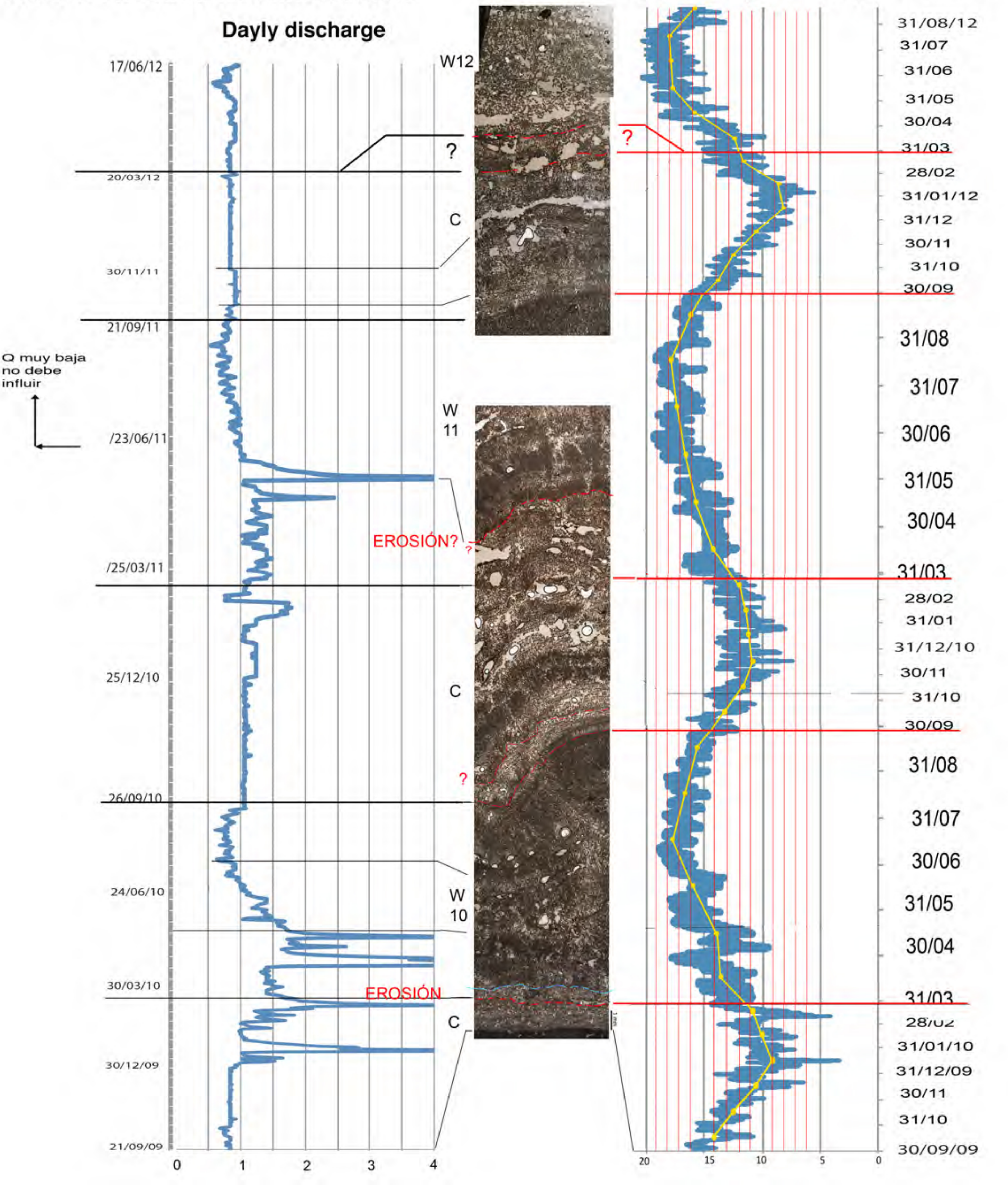

Table 1. Mean flow velocity, water depth and deposition rates obtained from November 1999 to September 2012 in sites with fast flow and stromatolite formation in the River Piedra (Compiled from Arenas et al., 2014). Cool = October to March period. Warm = April to September period. A: Stromatolites. C: Moss and algal boundstones.

Site	Studied period	Facies	Flow velocity (cm/s)		Water depth (cm)		Deposition rate (mm)		
			Cool	Warm	Cool	Warm	Mean of warm periods	Mean of cool periods	Mean yearly values
P-5	Apr 2003-Sept 2009	A	100.8	97.5	7.4	6.2	5.81	0.96	6.77
P-8	Apr 2003-Sept 2012	C +(A)	111.1	99.0	7.0	5.2	4.52	3.36	7.88
P-9	Oct 2006-Sept 2009	C +(A)	171.4	185.5	5.6	4.4	9.58	3.58	13.16
P-11	Nov 1999-Sept2012	C + A					6.48	3.80	10.29
P-12	Nov 1999-Sept2012	C +(A)					7.94	1.88	9.82
P-14	Nov 2000-Sept2012	A	227.7	221.5	7.4	6.5	9.82	6.20	16.02
P-16	Nov 1999-Sept2012	A	135.4	132.0	8.8	5.8	11.15	5.38	16.53
P-17	Apr 2000-Mar 2003	A	136.7	125.8			11.11	4.55	15.66
P-20	Nov 1999-Sept2012	A	180.2	165.9	7.3	5.8	9.83	4.97	14.80
Total mean							8.47	3.85	12.33
Mean A							9.54	4.41	13.96
Mean C+A							6.91	3.59	10.50

Table 2. Mean values of main hydrochemical characters of the studied sites with stromatolites in the River Piedra. A: Stromatolites. C: Moss and algal boundstones.

Sites	**Facies**	**Temp. (ºC)**		**Cond. (µS/cm)**		**Alkalinity (ppm HCO_3^-)**		**Ca (ppm)**		**pH**		**TDIC (ppm)**		**log pCO_2**		**SIc**		**PWP (mmol cm^{-2} s^{-1})**	
		Warm	Cool	Warm	Cool	Warm	Cool	Warm	Cool	Warm	Cool	Warm	Cool	Warm	Cool	Warm	Cool	Warm	Cool
P-5	A	17.6	9.8	631.0	677.2	263.3	285.7	85.8	87.3	8.15	7.96	51.6	57.5	-2.81	-2.62	0.86	0.61	2.76e-7	1.26e-7
P-8+9	C+A	17.3	9.6	643.5	640.8	286.1	288.9	90.6	88.4	8.09	7.86	56.3	59.0	-2.72	-2.53	0.86	0.51	2.75e-7	1.26e-7
P-11+12	C+A	17.2	9.0	643.9	650.5	264.9	271.8	85.9	89.9	8.14	8.07	52.0	54.4	-2.80	-2.76	0.85	0.68	2.61e-7	1.72e-7
P-14	A	16.9	9.5	654.0	654.6	269.0	273.5	87.6	89.1	8.18	8.09	52.6	54.7	-2.84	-2.78	0.89	0.72	3.13e-7	1.77e-7
P-16	A	17.2	9.1	623.9	636.0	262.5	266.4	82.5	84.3	8.20	7.97	51.2	53.8	-2.87	-2.67	0.89	0.57	2.78e-7	1.05e-7
P-20	A	17.2	9.5	639.6	640.7	265.0	270.1	86.8	88.5	8.32	8.24	51.1	53.0	-2.99	-2.94	1.02	0.85	3.68e-7	2.20e-7
Mean		17.2	9.4	639.3	650.0	268.5	276.1	86.5	87.9	8.18	8.03	52.5	55.4	-2.84	-2.72	0.89	0.66	2.95e-7	1.54e-7
Mean A		17.2	9.5	637.1	652.1	265.0	273.9	85.7	87.3	8.21	8.06	51.6	54.7	-2.88	-2.75	0.91	0.69	3.09e-7	1.57e-7
Mean C+A		17.2	9.3	643.7	645.6	275.5	280.3	88.2	89.2	8.11	7.96	54.1	56.7	-2.76	-2.64	0.85	0.59	2.68e-7	1.49e-7

Water samples taken in January and June: P-5: from June 2003 to June 2009 (n=13). P-8+9, P-16 and P-20: from June 2003 to June 2012 (n=19). P-11+12: from January 2001 to June 2012 (n=24). P-14: from September 1999 to June 2012 (n=27).

Type of lamina	Single lamina	Composite lamina	Main components
Dense	0.2 to 5 mm thick, consisting of micrite and spar calcite, formed of tightly-packed calcified filamentous microbes (calcite tubes). Semi-parallel tubes and/or fan-like structures. Microlamination. Low growth-framework porosity.	3.5 mm to 15 mm thick. Formed of up to 8 laminae that have undulatory and convex, less commonly flat bounding surfaces. Successive dense laminae and alternating thick dense and thin porous laminae. Porosity: up to 5 % (area).	Calcite tubes from encrustations of filamentous cyanobacteria (dominant *P. incrustatum*). Inner diameter: 6.0 to 7.5 µm Thickness of walls 3 to 8 µm thick, with calcite crystals up to 15 µm long.
Porous	0.5 to 2 mm thick, consisting of micrite and spar calcite, formed of loosly-packed calcified filamentous microbes (calcite tubes). Semi-parallel tubes and/or fan-like structures. Microlamination. High growth-framework porosity.	2 to 7.5 mm thick (exceptionally 12 mm). Formed of up to 5 laminae that have irregular and undulatory bounding surfaces. Alternating dense laminae and thicker porous laminae. Porosity: up to 15 % (area).	Matrix: Calcite crystals, diatoms, EPS, non-calcified bacterial filaments and and siliciclastics. In some cases, thicker tubes with smaller crystals in the dense laminae than in the porous laminae.
Macrocrys-talline	0.1 to 1.3 mm thick, made of closely packed elongate calcite macrocrystals that are (sub)perpendicular to the depositional surface and produce a fence-like structure. Low porosity (interparticle).	1 to 1.7 mm thick. Formed of 1 to 3 laminae that are of variable lateral extent and have sharp flat and convex-up bases and irregular, flat and convex-up tops.	Crystals, 0.1 to 1 mm long, with cone-like shape that widens upward. May include scattered calcite tubes between macrocrystals.